# SUPPLEMENTARY MATERIAL

FUTURE PATHWAYS FOR EVTOLS: A DESIGN OPTIMIZATION PERSPECTIVE

**Johannes Janning, Sophie F. Armanini, Urban Fasel**
Department of Aeronautics, Imperial College London, United Kingdom
{johannes.janning23, s.armanini, u.fasel}@imperial.ac.uk

## ABSTRACT

This supplemental documentation provides an in-depth technical description of the models and methodologies employed in the multidisciplinary co-design optimization framework for electric Vertical Take-Off and Landing (eVTOL) aircraft, as presented in the paper *"Future Pathways for eVTOL: A Design Optimization Framework."* The document elaborates on key components of the optimization framework, including mass, aerodynamic, power, energy, and economic models. It offers detailed insights into specific metrics such as maximum take-off mass (MTOM), battery performance, aerodynamic efficiencies, and operational costs. Additionally, it incorporates environmental considerations, with metrics such as Global Warming Potential (GWP), and addresses constraints related to wing-rotor geometries and operational infrastructure like vertiports. The framework integrates battery degradation models and operational cost assessments to facilitate the sustainable design and economic feasibility of eVTOL systems. This document serves as a comprehensive technical reference, supporting the implementation and validation of the proposed optimization methodology.

## Contents

**List of Figures** iv

**List of Tables** v

**Glossary** vi

**1 Key Design Metrics** 1

**2 Mass Model** 3

2.1 Maximum Take-Off Mass . . . 3
2.2 Battery Mass . . . 3
2.3 Payload . . . 3
2.4 Empty Mass . . . 4
2.4.1 Wing Mass . . . 4
2.4.2 Rotor Mass . . . 5
2.4.3 Landing Gear Mass . . . 6
2.4.4 Motor Mass . . . 7
2.4.5 Fuselage Mass . . . 8
2.4.6 Systems Mass . . . 9
2.4.7 Furnishing Mass . . . 9

**3 Aerodynamic Model** 11

3.1 Lift Model . . . 11
3.2 Drag Model . . . 11
3.3 Airfoil Data . . . 13

**4 Force Balance, Power & Energy Model** 15

4.1 Aircraft Efficiencies . . . 15
4.2 Momentum Theory Power Model . . . 15
4.2.1 Hover Power Required: . . . 15
4.2.2 Climb Power Required: . . . 16
4.2.3 Cruise Power Required: . . . 17
4.3 Energy Requirements . . . 18

**5 Economic Model** 20

5.1 Operations Model . . . 20
5.2 Operational Cost Model . . . 21
5.2.1 Total Operating Cost . . . 21
5.2.2 Cash Operating Cost . . . 22
5.2.3 Cost of Ownership . . . 25
5.2.4 Indirect Operating Cost . . . 26

5.3 Revenue and Profitability Model . . . . . 27

**6 Battery Degradation Model** **27**

6.1 Method 1: Empirical Model . . . . . 28

6.2 Method 2: Static Degradation . . . . . 29

**7 Constraint Model** **30**

7.1 Rotor Noise Modeling . . . . . 30

7.1.1 Tonal Noise in Hover: Gutin–Deming Model . . . . . 30

7.1.2 Broadband Noise: SKM Model . . . . . 31

7.1.3 Assumptions Summary . . . . . 32

7.1.4 Limitations . . . . . 32

7.2 Wing-Rotor Geometry Constraint . . . . . 32

7.3 Vertipad Constraint . . . . . 33

**8 Optimization Algorithm Analysis** **35**

8.1 Scope . . . . . 35

8.2 Gradient-based Algorithm (GBA) . . . . . 35

8.3 Genetic Algorithm (GA) . . . . . 35

8.4 GBA-GA Comparison . . . . . 35

8.5 Conclusion . . . . . 35

## List of Figures


1 Rotor mass model. . . . . 6
2 Motor architecture concept. . . . . 8
3 Airfoil data and regression models for NACA0012 and NACA2412. . . . . 12
4 Forces in climb. . . . . 16
5 Forces in climb. . . . . 16
6 Static Force Balance in Straight and Level Flight. . . . . 18
7 Operations Window. . . . . 20
8 Total operating cost structure. . . . . 22
9 Interpolated Curve for Cycle Life vs. DoD . . . . . 29
10 Piecewise Linear Fit for Cycle Life vs. DoD . . . . . 30
11 Hover SPL [dB(A)] from the Gutin–Deming model as a function of rotor radius and observer distance. 31
12 Geometry constraint on minimal wing span, lifting rotor and fuselage interference . . . . . 33
13 D-value for Vertiports. . . . . 34
14 Comparison of optimization performance between GA and GBO, illustrating objective function over function evaluations. . . . . 36
15 Boxplot comparison of FoM results from valid GBO and GA runs. . . . . 36

## List of Tables


1 Aircraft Design Key Metrics Overview. . . . . 1
2 Sustainability Key Metrics Overview. . . . . 1
3 Battery Design Key Metrics Overview. . . . . 2
4 Operational Key Metrics Overview. . . . . 2
5 Economic Key Metrics Overview. . . . . 3
6 Conversions from Metric to Imperial Units . . . . . 4
7 Technical Data for MT Propellers . . . . . 5
8 XFOIL polars for NACA 2412 at $Re = 4 \cdot 10^6$: lift, drag, moment, and transition locations. . . . . 13
9 XFOIL-generated polars for NACA 0012 at $Re = 4 \cdot 10^6$: lift, drag, moment, and transition locations. 14
10 System efficiencies. . . . . 15
11 Key acoustic model assumptions . . . . . 32
12 Gradient-based (SLSQP) results over 10 multi-start runs . . . . . 35
13 Genetic Algorithm (GA) results . . . . . 36

## Glossary

| | |
|---|---|
| $C_C$ | Crew Cost (€) |
| $C_E$ | Energy Cost (€) |
| $C_M$ | Maintenance Cost (€) |
| $C_N$ | Navigation Cost (€) |
| $C_T$ | Total Cycle Time Factor |
| $C_{dep}$ | Depreciation Cost (€) |
| $C_{ins}$ | Insurance Cost (€) |
| $C_{L\_climb}$ | Lift coefficient during climb |
| $C_{L\_cruise}$ | Lift coefficient during cruise |
| COC | Cash Operating Cost (€) |
| COO | Cost of Ownership (€) |
| CT | Total Cycle Time Factor |
| DOD | Depth of Discharge |
| $D_{climb}$ | Drag during climb (N) |
| $D_{cruise}$ | Drag during cruise (N) |
| $E_{BAT_{total}}$ | Total Battery Energy Storage Capacity |
| $E_{reserve}$ | Reserve energy required (Wh) |
| $E_{trip}$ | Trip energy required (Wh) |
| $E_{useable}$ | Usable energy (Wh) |
| $eBAT_{EOL}$ | End-of-life battery energy density (Wh/kg) |
| $FC_{annual}$ | Annual flight cycles |
| i | Interest Rate (%) |
| IOC | Indirect Operating Cost (€) |
| LF | Load Factor |
| MF | Maintenance Factor |
| $M_{battery}$ | Battery mass (kg) |
| $M_{empty}$ | Empty mass (kg) |
| MTOM | Maximum Take-Off Mass (kg) |
| $M_{payload}$ | Payload mass (kg) |
| MWR | Maintenance Wrap Rate |
| $n_{AC}$ | Number of Aircraft Controlled per Pilot |
| $N_{cycles}$ | Number of life cycles per battery |
| $P_{bats}$ | Battery Acquisition Cost per kWh |
| $P_{climb}$ | Power required during climb (W) |
| $P_{energy}$ | Energy price (C/kWh) |
| $P_{required\_hover}$ | Power required during hover (W) |
| RV | Residual Value (%) |
| SOC | State of Charge |
| SP | Pilot Salary (€) |
| $t_{trip}$ | Trip Time |
| TDA | Total Depreciation Amount (€) |
| $T_{req\_climb}$ | Thrust required during climb (N) |
| $T_{req\_cruise}$ | Thrust required during cruise (N) |
| $T_{required\_hover}$ | Thrust required during hover (N) |
| $T_D$ | Daily operation window (hours) |
| $T_T$ | Turnaround time (minutes) |
| TOC | Total Operating Cost (€) |
| $U_{pilot}$ | Annual Utilization of One Pilot |
| $V_{climb}$ | Climb speed (m/s) |
| $V_{cruise}$ | Cruise speed (m/s) |
| $v_i$ | Induced velocity (m/s) |
| $x_{ins}$ | Insurance Factor |
| $\eta_c$ | Cruise efficiency |
| $\eta_e$ | Electric efficiency |
| $\eta_h$ | Hover efficiency |
| $\eta_{hp}$ | Hover propulsive efficiency |
| $\eta_p$ | Propulsive efficiency |
| $\lambda_{trip}$ | Annual trip-time ratio |
| $\rho_{bat}$ | Battery energy density (Wh/kg) |
| $\sigma$ | Propeller disk loading (N/m²) |

# 1 Key Design Metrics

| Key Metrics | Description |
|---|---|
| **MTOM** ($kg$) | Crucial metric that represents the total mass the aircraft is designed to carry, including the aircraft itself, passengers, cargo, and batteries. It directly impacts performance, range, and regulatory compliance. |
| **Empty Mass** ($kg$) | Includes the weight of the aircraft without any payload or battery. A lower empty mass generally indicates a more efficient design, potentially allowing for more payload or longer range and reduced aircraft acquisition cost. |
| **Wing Mass** ($kg$) | Contributes significantly to the overall structural weight. It affects the aircraft's balance, structural integrity, and aerodynamic performance. Optimizing wing mass is crucial for maintaining a balance between strength and weight efficiency. |
| **Battery Mass** ($kg$) | Critical in electric aircraft, as it directly impacts range, endurance, and overall energy efficiency. A heavier battery can provide more energy but may reduce efficiency and payload capacity. |
| **Aspect Ratio** ($-$) | Key indicator of aerodynamic efficiency. A higher aspect ratio typically leads to lower drag, improving fuel efficiency and range. |
| **Wing Loading** ($kg/m^2$) | Affects the aircraft's performance in terms of takeoff, landing, and maneuverability. It's a critical factor in determining how the aircraft behaves under different flight conditions. |
| **Disk Loading** ($kg/m^2$) | Important for vertical take-off and landing (VTOL) performance. Lower disk loading generally improves hover efficiency and reduces the power required for lift. |

Table 1: Aircraft Design Key Metrics Overview.

| Key Metrics | Description |
|---|---|
| **GWP per Flight** ($CO2_e kg$) | Measures the total CO2 equivalent emissions generated by the aircraft during a single flight. It's crucial for assessing the direct environmental impact of each operation, allowing to evaluate how sustainable each design is on a per-flight basis, providing a clear understanding of the environmental footprint of individual operations. |
| **GWP per Year** ($CO2_e kg$) | Aggregates the total CO2 equivalent emissions for all flights over a year. It's essential for understanding the long-term environmental impact of the eVTOL operations for evaluating sustainability in the context of regulatory compliance and corporate environmental goals. |
| **GWP per Passenger Kilometer** ($CO2_e kg/km$) | Normalizes the CO2 emissions by the distance traveled per passenger, making it easier to compare the environmental efficiency of different designs or transportation modes. |
| **Energy per Kilometer (EpK)** ($kWh/km$) | Measures the energy consumption of the eVTOL per kilometer traveled, allowing to assess how different designs optimize energy use, which is critical for both sustainability and cost efficiency. |
| **Charging C-rate** ($1/h$) | Indicates how quickly the battery can be recharged. Faster charging times are crucial for reducing turnaround times in operations but may affect battery longevity if not managed properly. |
| **Trip Energy Required** ($Wh$) | Measures the total energy consumed during a single flight. It's a comprehensive metric that captures the energy demands of the entire operation, from takeoff to landing, providing a holistic view of the energy efficiency of each flight. |

Table 2: Sustainability Key Metrics Overview.

| Key Metrics | Description |
|---|---|
| **Battery Density** ($Wh/kg$) | Measures how much energy a battery can store relative to its weight. Higher energy density is desirable because it allows for longer flight times and greater range without significantly increasing the aircraft's weight. |
| **Battery Capacity** ($kWh$) | Determines the total amount of energy available for a flight. It directly impacts the range and endurance of the eVTOL. A higher capacity allows for longer trips but usually results in a heavier battery, affecting overall efficiency. |
| **Depth of Discharge (DoD)**($\%$) | Indicates the percentage of the battery's total capacity that is used during a discharge cycle. Managing DoD is crucial for balancing range with battery longevity; deeper discharges can shorten battery life, while shallower discharges may limit range. |
| **Average Discharge C-rate** ($1/h$) | Measures how quickly a battery is discharged relative to its capacity. The average discharge C-rate provides insight into the battery's performance during a typical flight. High C-rates can stress the battery, potentially reducing its lifespan, but may be necessary for high power demands. |
| **Charging C-rate** ($1/h$) | Indicates how quickly the battery can be recharged. Faster charging times are crucial for reducing turnaround times in operations but may affect battery longevity if not managed properly. |
| **Number of Battery Cycles** ($-$) | Measures the number of complete charge/discharge cycles the battery can undergo before its capacity significantly degrades. It's a critical factor in determining the overall lifespan of the battery and impacts the cost-efficiency of operations. |
| **Number of Yearly Required Batteries** ($-$) | Estimates how many batteries are needed per year to maintain operations, accounting for factors like battery wear and the number of cycles. It's essential for understanding operational costs, planning maintenance and estimating total global warming potential (GWP) of the eVTOL operation, due battery lifecycle environmental impact. |
| **Battery Unit Cost (€)** | Key economic metric that influences the overall maintenance cost and operation. Lower battery costs are preferable, especially if batteries need frequent replacement. |

Table 3: Battery Design Key Metrics Overview.

| Key Metrics | Description |
|---|---|
| **Flight Cycles per Day** ($-$) | Measures the number of complete flights an eVTOL can perform daily while indicates daily operational capacity and utilization; higher values suggest better efficiency. |
| **Flight Cycles per Year** ($-$) | Total number of flights over a year. Reflects long-term operational workload, impacting maintenance and lifecycle costs. |
| **Flight Hours per Day** ($hrs$) | Total time the eVTOL spends in the air each day, providing a measure of daily operational tempo and productivity. |
| **Flight Hours per Year** ($hrs$) | Aggregated flight time over a year. Key for planning maintenance and understanding long-term aircraft usage. |
| **Travel Time** ($min$) | Total time for a complete trip, including takeoff, cruise, and landing. Shorter travel times may improve customer satisfaction and operational efficiency. |
| **Turnaround Time Between Trips** ($min$) | Assumed as time needed to prepare the eVTOL for the next flight, including charging. Shorter turnaround times maximize flight availability and operational efficiency. |
| **Cruise Speed** ($km/h$) | Directly impacts the duration of the flight, the efficiency of the operation, and the scheduling of trips. It affects how quickly the eVTOL can complete a journey, which in turn influences the number of trips it can perform within a given time period and also determines eVTOL power requirements. |
| **Power in Hover** ($kW$) | Measures the power required to maintain a hover, critical for VTOL operations, crucial for urban operations. |
| **Power in Climb** ($kW$) | Measures the power needed during the climb phase, which is typically energy-intensive. |
| **Power in Cruise** ($kW$) | Measures the power required to maintain cruise speed. It's crucial for understanding energy efficiency during the longest phase of flight. |

Table 4: Operational Key Metrics Overview.

| Key Metrics | Description |
|---|---|
| **Total Operating Cost (€)** | Captures all costs associated with operating the eVTOL for one trip, providing an overall measure of economic efficiency per flight. |
| **Cash Operating Cost (€)** | Focuses on the cash expenses incurred during each flight. Useful for understanding immediate financial outflows directly related to eVTOL operation. |
| **Energy Cost (€)** | The cost of energy consumed during a single trip, directly linked to the aircraft's energy efficiency and the operator's regional electricity mixture network. |
| **Warp Rated Maintenance (€)** | Estimated maintenance costs, considering wear and tear per trip. |
| **Battery Replacement Cost (€)** | Cost allocated for battery replacement, spread over the battery's life. |
| **Navigation Cost (€)** | Expenses related to navigation services during the flight, containing air traffic service charges. |
| **Crew Cost (€)** | Wages for the flight crew per trip. |
| **Cost of Ownership (€)** | Total cost of owning and operating the eVTOL, divided per trip. Provides a comprehensive view of long-term financial commitments. |
| **Aircraft Price (€)** | Estimated initial purchase price of the eVTOL. Key for calculating depreciation and understanding capital investment. |
| **Profit per Flight (€)** | Revenue minus costs for each flight. Direct measure of economic performance per operation. |
| **Annual Profit (€)** | Total profit accumulated over a year. Crucial for assessing the long-term viability and success of the eVTOL operation, depending on operational metrics. |

Table 5: Economic Key Metrics Overview.

# 2 Mass Model

## 2.1 Maximum Take-Off Mass

**Assumptions and Limitations:**

- Due to the preliminary design nature of the optimization, MTOM should be treated as a first estimate.
- The proposed design optimization allows a deviation by 2% of Eq. 1.

The total mass of an eVTOL aircraft can be described by:

$$MTOM = M_{payload} + M_{empty} + M_{battery} \leq Limit_{certification} \tag{1}$$

with $MTOM$ being the maximum take-off mass, $M_{payload}$ the payload mass, $M_{empty}$ the empty mass, and $M_{battery}$ the battery mass, in kg. According EASA's latest certification specifications for eVTOL, Ref. [1], the maximum certifiable weight is limited to $Limit_{certification} = 5.700kg$.

## 2.2 Battery Mass

**Assumptions and Limitations:**

- Battery Mass accounts for design mission energy requirements, as sum of reserve and trip energy. Reserve energy can be adjusted by the user by selecting reserve time, which is assumed to be 30min in cruise power.
- 20% of unusable battery capacity in terms of state of charge ceiling and floor are considered (see Chapter 4.3).
- The end-of-life battery status is considered, defined by 80% of begin-of-life condition (see Chapter 4.3).

Historically, $M_{battery}$ would be considered as part of $M_{empty}$, but for enormous impact of $M_{battery}$ on MTOM, it is considered separately. $M_{battery}$ can be calculated by Eq. 2, considering the design mission energy needs and battery energy density $\rho_{bat}$ in Wh/kg. The factor of $0.64$ accounts for unusable battery energy (see Chapter 4.3).

$$M_{battery} = \frac{E_{useable}}{e_{usable}} = \frac{E_{trip} + E_{res}}{0.64 \cdot \rho_{bat}} \, [kg] \tag{2}$$

## 2.3 Payload

**Assumptions and Limitations:**

- Payload is defined by load factor, number of passengers and their average mass.
- Within this framework a constant payload and a load factor of 1 is considered, according Eq. 4.

$M_{payload}$ should count for an average passenger weight $M_{pax}$ and luggage weight per passenger $M_{lug}$. The mean Passenger and Luggage weights for commercial air transportation are assumed $M_{pax}$=82.2kg and $M_{lug}$=16kg [2]. $n_{seats}$ is the maximum seat capacity of the aircraft. LF is the load factor of the aircraft.

$$M_{payload} = (M_{pax} + M_{lug}) \cdot n_{seats} \cdot LF \tag{3}$$

In a fully loaded 4-seater eVTOL this results in:

$$M_{payload} = (82.2 + 16) \cdot 4 \cdot 1 = 392.8\,[kg] \tag{4}$$

### 2.4 Empty Mass

**Assumptions and Limitations:**

- This method is used within the presented optimization.
- Statistical methods highly depend on the used data set for model fit. The provided methods are based on general aviation aircraft.
- The provided equations are highly unit sensitive. Use the provided conversion table to transfer metric units into imperial units, insert the imperial units into the models and re-transfer the results from pounds to kilogram.
- Wihtin this framework, statistical mass estimations according Raymer [3] and Nicolai [4] are averaged.

The empty mass in this method is defined as:

$$M_{empty} = M_{wing} + M_{rotor} + M_{motor} + M_{fuselage} + M_{systems} + M_{furnish} + M_{crew} \tag{5}$$

Where crew mass $M_{crew}$ is based on average masses for single pilot operation [2]. Within this method, the values in Table 6 are used for unit conversion.

| Unit | Metric | Imperial |
|---|---|---|
| Weight | 1 kg | 2.20462 lb |
| Length | 1 m | 3.28084 ft |
| Area | 1 $m^2$ | 10.7639 $ft^2$ |
| Speed | 1 m/s | 1.94384 kt |

Table 6: Conversions from Metric to Imperial Units

#### 2.4.1 Wing Mass

**Assumptions and Limitations:**

- Within optimization model, rectangular wing with NACA2412 airfoil is assumed, taper ratio $\lambda$ is assumed 1 and sweep angle $\Lambda_{c/4}$ to be 0°.
- Airfoil data for NACA0012 is provided in Chapter 3 and can be adjusted in the provided optimization code.
- Thickness to chord $t/c$ ratio is assumed for 0.12 (NACA2412).
- Maximum level airspeed $V_H$ is assumed to equal $V_{cruise}$.
- The calculation of the wing mass is based solely on statistical mass estimation, based on historical aircraft data from general aviation. Detailed structural and geometric characteristics of the wings are not taken into account. The integration of a FEM model, for example, for a more accurate calculation of the wing mass, taking into account more precise wing design parameters, has the potential to significantly complement the proposed model in future work.

**Raymer:**

$$M_{W_R} = 0.036 \cdot S_W^{0.758} W_{FW}^{-0.0035} \left(\frac{AR_W}{\cos^2 \Lambda_{C/4}}\right)^{0.6} q^{0.006} \lambda^{0.04} \left(\frac{100 \cdot t/c}{\cos \Lambda_{C/4}}\right)^{-0.3} (n_z W_O)^{0.49} \tag{6}$$

**Nicolai:**

$$M_{W_N} = 96.948 \cdot \left(\frac{n_z W_O}{10^5}\right)^{0.65} \left(\frac{AR_W}{\cos^2 \Lambda_{C/4}}\right)^{0.57} \left(\frac{S_W}{100}\right)^{0.61} \left(\frac{1+\lambda}{2(t/c)}\right)^{0.36} \left(\sqrt{1+\frac{V_H}{500}}\right)^{0.993} \tag{7}$$

In the given equations:

- $M_W$ is the predicted weight of the wing in pounds-force (lbf).
- $S_W$ is the trapezoidal wing area in square feet (ft$^2$).
- $W_{FW}$ is the weight of fuel in the wing in pounds (lbs) (if $W_{FW} = 0$, then let $W_{FW}^{0.0035} = 1$).
- $AR$ denotes the Aspect Ratio of the wing, HT, or VT, as per the appropriate subscripts.
- $\Lambda_{C/4}$ is the wing sweep at 25% Mean Geometric Chord (MGC).
- $q$ represents the dynamic pressure at cruise.
- $\lambda$ is the wing taper ratio.
- $t/c$ refers to the wing thickness to chord ratio.
- $n_z$ is the ultimate load factor.
- $W_0$ is the design gross weight in pounds (lbs).
- $V_H$ is the maximum level airspeed at Sea Level (S-L) in Knots Equivalent Airspeed (KEAS).

Resulting in:

$$M_{wing} = \frac{M_{W_R} + M_{W_N}}{2} \tag{8}$$

### 2.4.2 Rotor Mass

The rotor weight model from [5], which deals with UAM, was adopted and adapted for passenger transporting eVTOL using a correction factor. The average weight and radius of a series of MT propellers from Table 7, based on [6], was used as a reference to identify a matchpoint where the radius of 1.1m hits 18.0kg. In addition the model was damped by adjusting the potency of the disproportionality to moderate the exponential increase in rotor weight with rotor size.

$$M_R = k_{rotor} \cdot \left[n_h \cdot \left(0.7484 \cdot R_{\text{hover}}^{1.2} - 0.0403 \cdot R_{\text{hover}}\right) + n_c \cdot \left(0.7484 \cdot R_{\text{cruise}}^{1.2} - 0.0403 \cdot R_{\text{cruise}}\right)\right] \tag{9}$$

where $n_h$ and $n_c$ are the number of rotors in the hover configuration and cruise configuration, respectively. The empirical scaling constant for eVTOL rotor mass was selected as $k_{rotor} = 22.649$. The average mass per propeller can be obtained by dividing the total rotor mass $M_R$ by the total number of propellers:

$$M_{\text{rotor, per unit}} = \frac{M_R}{n_h + n_c}. \tag{10}$$

During climb, the cruise propeller is used. $R_i$ represents the radius of each propeller, with $i$ indicating either the hover or cruise configuration. This model relies on empirical scaling of propeller data and correction factors, and therefore does not account for detailed structural design choices, material properties, or manufacturing constraints, which may affect rotor mass particularly outside the calibrated size range.

| **Type** | **MT-11** | **MT-15** | **MTV-21** | **MTV-17** | **MTV-20** | **Average** |
|---|---|---|---|---|---|---|
| **D [cm]** | 190 | 260 | 203 | 190 | 210 | |
| **r [cm]** | 95 | 130 | 101.5 | 95 | 105 | 1.1 |
| **M [kg]** | 16 | 25 | 12 | 16 | 21 | 18 |

Table 7: Technical Data for MT Propellers

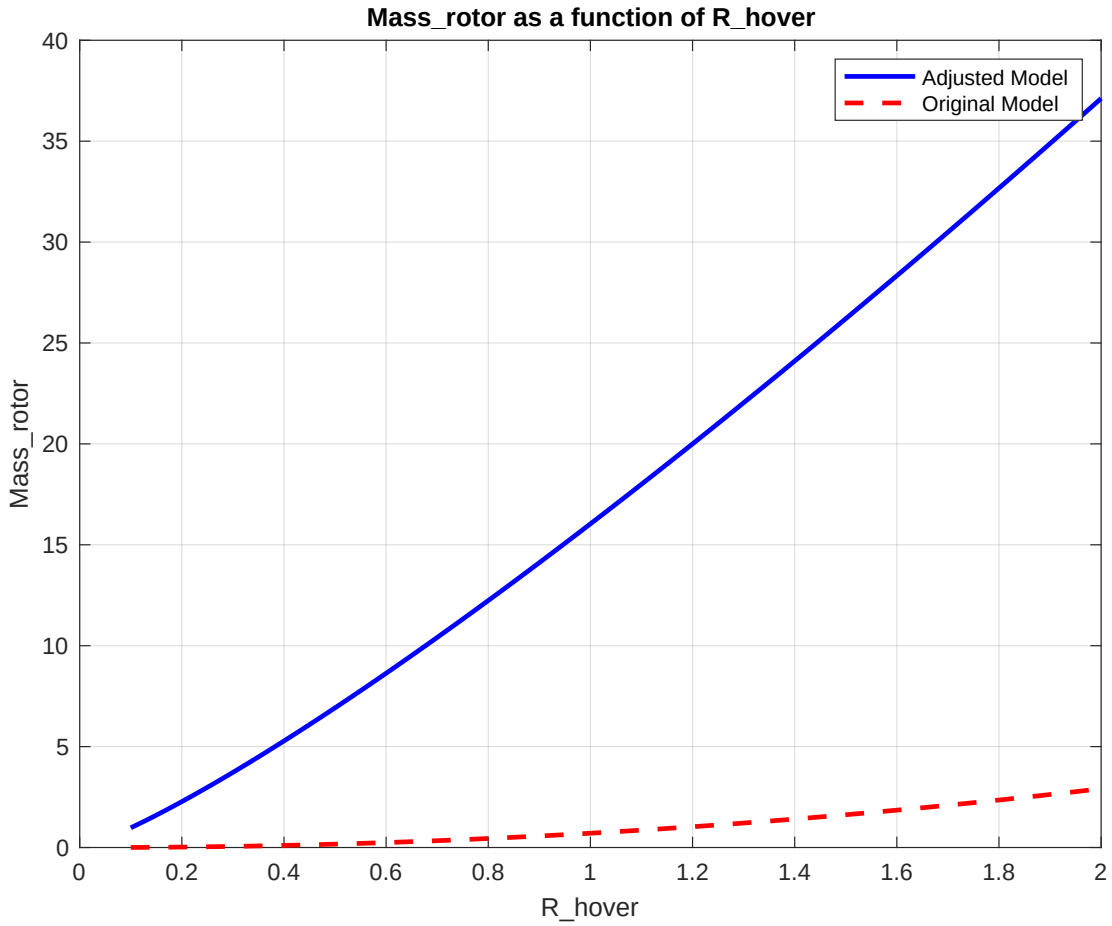


Figure 1: Rotor mass model.

### 2.4.3 Landing Gear Mass

**Assumptions and Limitations:**

- The provided equations are highly unit sensitive. Use the provided conversion table to transfer metric units into imperial units, insert the imperial units into the models and re-transfer the results from pounds to kilogram.

The Landing gear mass is computed by averaging statistical models. Raymer provides to equations, one for main landing gear and one for nose landing gear. Nicolai provides a model for the entire landing gear. The landing gear weight is driven by total aircraft mass $MTOM$ and length of the gear struts $L_m$ and $L_n$, summarized as $L_i$. $L_i$ is defined by the cruise propeller radius $R_{prop_{cruise}}$ and the minimum propeller clearance of 7 inches (0.1778m) as required by EASA, Ref. [7], and FAA, Ref. [8].

**Raymer:**

$$W_{MLG_R} = 0.095 \cdot (n_l \cdot W_l)^{0.768} \left(\frac{L_m}{12}\right)^{0.409} \tag{11}$$

$$M_{NLG_R} = 0.125 \cdot (n_l W_l)^{0.566} \left(\frac{L_n}{12}\right)^{0.845} \tag{12}$$

where:

- $W_{\text{MLG}}$ = predicted weight of the main landing gear in lbf.

- $W_{\text{NLG}}$ = predicted weight of the nose landing gear in lbf.
- $n_l$ = ultimate landing load factor (set to $1.5 \cdot 2.5 = 3.75$, with $2.5$ as maximum load factor $1.5$ as safety factor).
- $L_m$ = length of the main landing gear strut in inches.
- $W_l$ = design landing weight in lbf.
- $L_n$ = length of the nose landing gear strut in inches.

**Nicolai:**

$$M_{MNLG_N} = 0.054 \cdot (n_l W_l)^{0.684} \left(\frac{L_m}{12}\right)^{0.601} \tag{13}$$

where:

- $n_l$ = ultimate landing load factor.
- $W_l$ = design landing weight in lbf.
- $L_m$ = length of the main landing gear strut in inches.
- $W_{\text{MNLG}}$ = predicted weight of the entire landing gear in lbf.

Resulting in:

$$M_{gear} = \frac{M_{MLG_R} + M_{NLG_R} + M_{MNLG_N}}{2} \tag{14}$$

#### 2.4.4 Motor Mass

**Assumptions and Limitations:**

- The motor mass model, based on Ref. [9], is valid for the power range from 10 kW to 260 kW per motor.
- A power sizing margin factor of $s = 1.5$ is applied to ensure that available power exceeds required power ($P_{\text{available}} \geq P_{\text{required}}$) across all design-mission segments. This factor accounts for transients, installation overhead, operational derating, and certification reserves.

The model is based on Ref. [9] and depends on the number of motors, which is set to the number of rotors, aligning with the power architecture of the eVTOL shown in Fig. 2.

$$M_{motor} = n_h \cdot 0.6756 \left(\frac{s \cdot P_{\text{hover,req}}}{n_h \cdot 745.7}\right)^{0.783} + n_c \cdot 0.6756 \left(\frac{s \cdot P_{\text{climb,req}}}{n_c \cdot 745.7}\right)^{0.783} \tag{15}$$

where $P_{\text{hover,req}}$ and $P_{\text{climb,req}}$ are the required mission powers in hover and climb, respectively, $s = 2.5$ is the power sizing margin, and the output is the estimated motor mass in kilograms (kg). $n_h$ and $n_c$ are the number of rotors in the hover and cruise configuration, respectively.

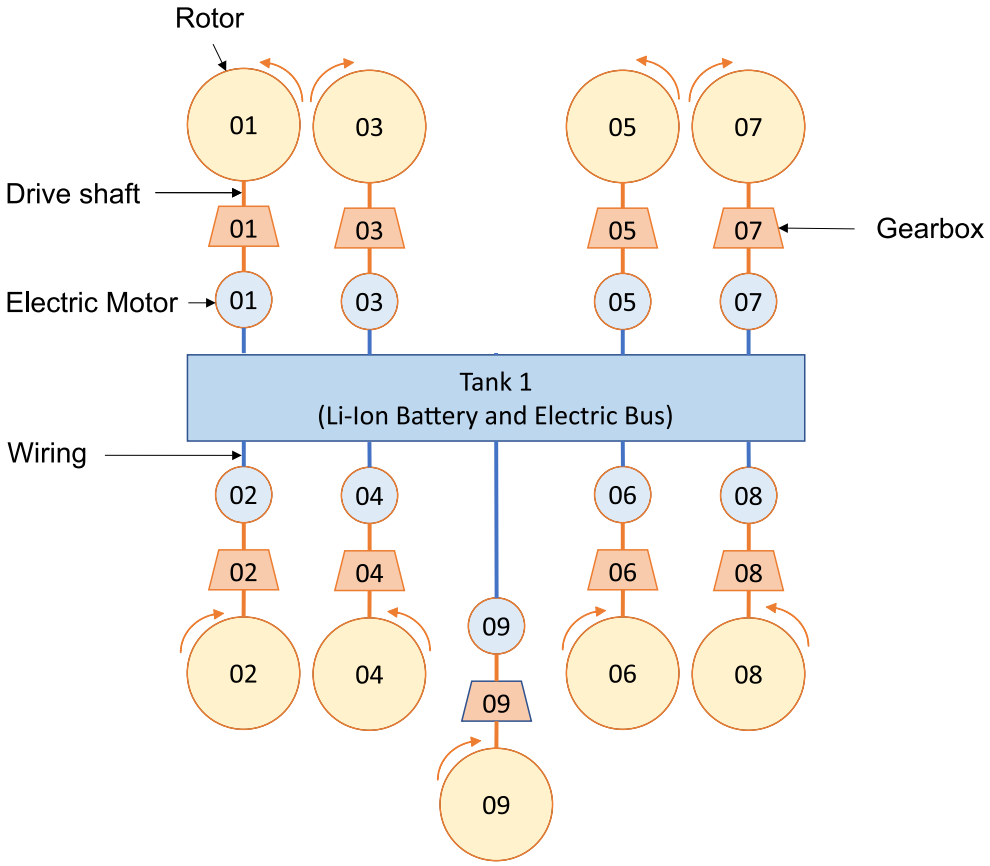


Figure 2: Motor architecture concept, from Ref. [10].

### 2.4.5 Fuselage Mass

**Assumptions and Limitations:**

- The provided equations are highly unit sensitive. Use the provided conversion table to transfer metric units into imperial units, insert the imperial units into the models and re-transfer the results from pounds to kilogram.
- The calculation of the fuselage mass is based on statistical mass estimation methods. The structural and geometric properties of the stringers, frames and skins are NOT taken into account. Consideration of the structural calculation may contribute to a significant future extension of the model.

The fuselage mass accounts for the structural mass of the frames, stringer, and skin of the main fuselage.

**Raymer:**

$$W_{\text{FUS}} = 0.052 \cdot S_{\text{FUS}}^{0.086} \cdot (n_z W_0)^{0.177} l_{\text{HT}}^{-0.051} \left(\frac{l_{\text{FS}}}{d_{\text{FS}}}\right)^{-0.072} q^{0.241} + 11.9 \cdot (V_P \Delta P)^{0.271} \tag{16}$$

**Nicolai:**

$$W_{\text{FUS}} = 200 \left[ \left(\frac{n_z W_0}{10^5}\right)^{0.286} \left(\frac{l_F}{10}\right)^{0.857} \left(\frac{w_F + d_F}{10}\right) \left(\frac{V_H}{100}\right)^{0.338} \right]^{1.1} \tag{17}$$

where:

- $W_{\text{FUS}}$ = predicted weight of the fuselage in lbf.

- $S_{\text{FUS}}$ = fuselage wetted area in ft$^2$.
- $l_{\text{FS}}$ = length of fuselage structure (forward bulkhead to aft frame) in ft.
- $d_{\text{FS}}$ = depth of fuselage structure in ft.
- $V_P$ = volume of pressurized cabin section in ft$^3$.
- $\Delta P$ = cabin pressure differential, in psi (typically 8 psi).
- $l_F$ = fuselage length in ft.
- $w_F$ = fuselage max width in ft.
- $d_F$ = fuselage max depth in ft.
- $l_{\text{HT}}$ = length of fuselage structure.
- $n_z$ = ultimate load factor.
- $W_0$ = design gross weight in lbf.
- $q$ = dynamic pressure at cruise.
- $V_H$ = maximum level airspeed at sea level (S-L) in knots equivalent airspeed (KEAS).

#### 2.4.6 Systems Mass

**Assumptions and Limitations:**

- The provided equations are highly unit sensitive. Use the provided conversion table to transfer metric units into imperial units, insert the imperial units into the models and re-transfer the results from pounds to kilogram.

The systems mass accounts for the flight control system and avionics. We assume it also covers air conditioning, lights and other non-flying electronics.

**Raymer:**

$$M_{system_R} = 0.053 \cdot l_{\text{FS}}^{1.536} \cdot b^{0.371} \cdot \left(n_z W_0 \cdot 10^{-4}\right)^{0.80} \tag{18}$$

**Nicolai:**

$$M_{system_N} = 1.08 W_0^{0.7} \tag{19}$$

where:

- $W_{\text{CTRL}}$ = predicted weight of the flight control system in lbf.
- $l_{\text{FS}}$ = length of fuselage structure in ft.
- $b$ = wingspan in ft.
- $n_z$ = ultimate load factor.
- $W_0$ = design gross weight in lbf.

Resulting in:

$$M_{system} = \frac{M_{system_R} + M_{system_N}}{2} \tag{20}$$

#### 2.4.7 Furnishing Mass

**Assumptions and Limitations:**

- The provided equations are highly unit sensitive. Use the provided conversion table to transfer metric units into imperial units, insert the imperial units into the models and re-transfer the results from pounds to kilogram.

The furnish mass accounts for interior of the eVTOL, like seating and other travel-experience related equipment like entertainment.

**Raymer:**

$$M_{furn_R} = 0.0582 W_0 - 65 \tag{21}$$

**Nicolai:**

$$M_{furn_N} = 34.5 N_{\text{CREW}} q_H^{0.25} \tag{22}$$

where:

- $W_{\text{FURN}}$ = predicted weight of furnishings in lbf.
- $W_0$ = design gross weight (maximum take-off mass, MTOM) in lbf.
- $N_{\text{CREW}}$ = number of crew.
- $q_H$ = dynamic pressure at max level airspeed, in lbf/ft$^2$.

Resulting in:

$$M_{furnish} = \frac{M_{furn_R} + M_{furn_N}}{2} \tag{23}$$

## 3 Aerodynamic Model

In this model we use a simplified aerodynamic lift and drag model to calculate lift coefficient $C_L$ and drag coefficient $C_D$ of the eVTOL wing, based on Ref. [11] and Ref. [12]. The airfoil data is taken from Ref. [13] at $Re = 200,000$.

### 3.1 Lift Model

Within this framework only the pre-stall aerodynamics are considered. A linear pre-stall lift curve is assumed with a stall angle of attack at 15°. According [12], the finite-wing-lift-curve slope $\alpha_{wing}$ is described by:

$$\alpha_{wing} = \frac{\alpha_{airfoil}}{1 + \frac{\alpha_{airfoil}}{\pi \cdot AR \cdot e}} \tag{24}$$

where $AR$ is the wing aspect ratio, $e$ is the oswald span efficiency, set to 0.8, and $\alpha_{airfoil}$ is the airfoil-lift-curve slope. During the development of this model there are two airfoil profiles in consideration. Based on Ref. [12] and in the interest of simplicity the symmetric NACA 0012 profile (0% camber, 12% max thickness at 30% chord, Ref. [12]) can be used. To simulate an airfoil with camber, the NACA 2412 can be used as it provides more lift at lower angle of attacks compared to the NACA 0012 (2% max camber at 40% chord, 12% max thickness at 30% chord, Ref. [12]), making it more efficient in urban and regional air mobility. The finite-wing lift coefficient model is defined as:

$$C_L = \frac{\alpha_{airfoil}}{1 + \frac{\alpha_{airfoil}}{\pi \cdot AR \cdot e}} \cdot \alpha + C_{L_0} = \alpha_{wing} \cdot \alpha + C_{L_0} \tag{25}$$

where $C_{L_0}$ is the lift coefficient at zero angle of attack (equals 0 for NACA 0012) and $\alpha$ is the angle of attack. The Reynolds number is estimated from the free-stream velocity $V$, the chord length $c$, and the kinematic viscosity $\nu$ of air. With $V \approx 60\ \mathrm{m/s}$, $c = 1\ \mathrm{m}$, and $\nu \approx 1.46 \times 10^{-5}\ \mathrm{m^2/s}$ (standard sea-level conditions), we obtain:

$$Re = \frac{V\,c}{\nu} = \frac{60 \cdot 1}{1.46 \times 10^{-5}} = 4.109 \times 10^6 \approx 4 \times 10^6 \tag{26}$$

The slope of the lift coefficient of the airfoil NACA 0012 and NACA 2412 are computed with linear regression using the data from Table 9 and 8.

$$\text{NACA0012} : C_L = 0.1089(1/deg) \cdot \alpha(deg) = 6.239(1/rad) \cdot \alpha(rad) \tag{27}$$

$$\text{NACA2412} : C_L = 0.1003(1/deg) \cdot \alpha(deg) + 0.2834 = 5.747(1/rad) \cdot \alpha(rad) + 0.2834 \tag{28}$$

This results in total lift, where $\rho$ is the air density, $V$ is the aircraft's true air speed, $S$ is the wings reference area:

$$L = \frac{1}{2} \cdot \rho \cdot V^2 \cdot S \cdot C_L = \frac{1}{2} \cdot \rho \cdot V^2 \cdot S \cdot \left( \frac{\alpha_{airfoil}}{1 + \frac{\alpha_{airfoil}}{\pi \cdot AR \cdot e}} \cdot \alpha + C_{L_0} \right) \tag{29}$$

### 3.2 Drag Model

The model used is based on the lifting line theroy [12] and assumes finite-wing-drag coefficient as composition of induced drag $C_{D_i}$ and parasite drag $C_{D_{min}}$:

$$C_D = C_{D_{min}} + C_{D_i} \tag{30}$$

with

$$C_{D_i} = \frac{C_L^2}{\pi \cdot AR \cdot e} \tag{31}$$

and $C_{D_{min}} = 0.0397$ based on the approach by Ref. [5] and the wind-tunnel experiments of Ref.[14], accounting for additional drag of the lifting rotors of a lift+cruise configuration. Resulting in following drag model:

$$C_D = 0.0397 + \frac{C_L^2}{\pi \cdot AR \cdot e} \tag{32}$$

and total drag:

$$D = \frac{1}{2} \cdot \rho \cdot V^2 \cdot S \cdot C_D = \frac{1}{2} \cdot \rho \cdot V^2 \cdot S \cdot \left( 0.0397 + \frac{C_L^2}{\pi \cdot AR \cdot e} \right) \tag{33}$$

The resulting lift and drag coefficient models are shown in Fig. 3. Within the model, a constant angle of attack during climb $\alpha_{climb} = 8°$ and $\alpha_{climb} = 3°$ is assumed, to account for realistic operational conditions.

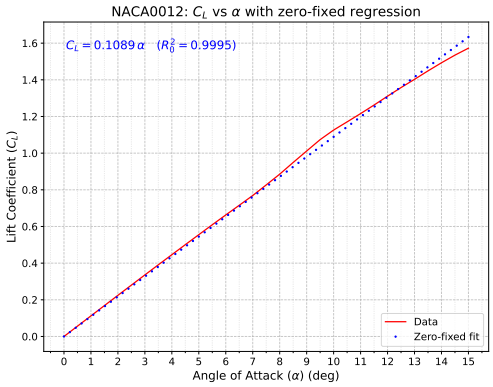


(a) Lift coefficient model for NACA0012.

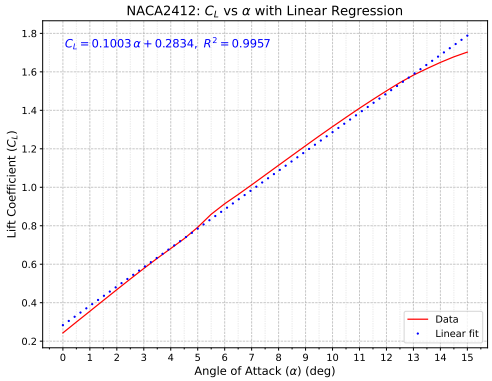


(b) Lift coefficient model for NACA2412.

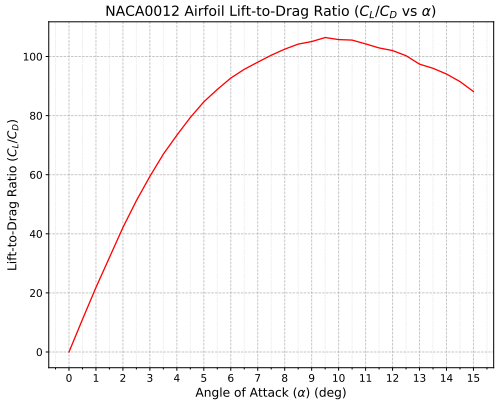


(c) Drag coefficient model for NACA0012.

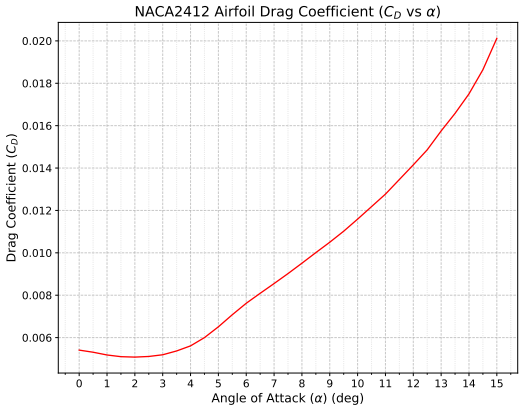


(d) Drag coefficient model for NACA2412.

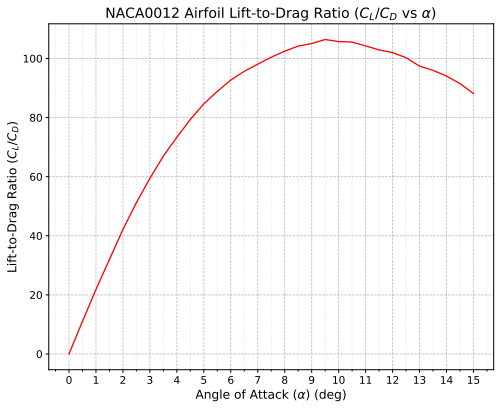


(e) Lift-to-drag ratio model for NACA0012.

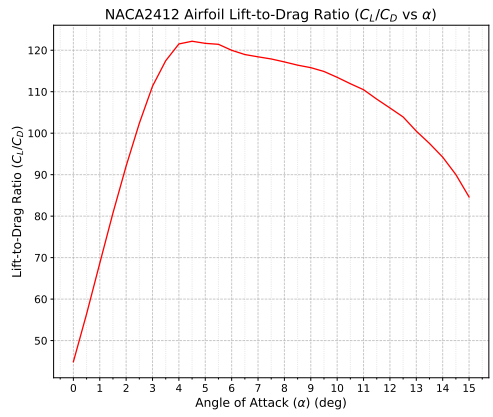


(f) Lift-to-drag ratio model for NACA2412.

Figure 3: Airfoil data and regression models for NACA0012 and NACA2412.

### 3.3 Airfoil Data

NACA 2412 data generated with XFOIL [15].

| $\alpha_{\text{deg}}$ | $C_L$ | $C_D$ | $C_{Dp}$ | $C_M$ | Top_Xtr | Bot_Xtr |
|---|---|---|---|---|---|---|
| 0.0 | 0.2429 | 0.00541 | 0.00075 | -0.0528 | 0.4979 | 0.3444 |
| 0.5 | 0.2995 | 0.00531 | 0.00077 | -0.0530 | 0.4739 | 0.4130 |
| 1.0 | 0.3555 | 0.00518 | 0.00081 | -0.0530 | 0.4490 | 0.5089 |
| 1.5 | 0.4118 | 0.00510 | 0.00087 | -0.0531 | 0.4267 | 0.5903 |
| 2.0 | 0.4678 | 0.00508 | 0.00096 | -0.0531 | 0.4002 | 0.6680 |
| 2.5 | 0.5232 | 0.00511 | 0.00108 | -0.0530 | 0.3682 | 0.7450 |
| 3.0 | 0.5778 | 0.00519 | 0.00123 | -0.0527 | 0.3327 | 0.8207 |
| 3.5 | 0.6308 | 0.00537 | 0.00143 | -0.0521 | 0.2915 | 0.8904 |
| 4.0 | 0.6817 | 0.00561 | 0.00166 | -0.0509 | 0.2512 | 0.9459 |
| 4.5 | 0.7330 | 0.00600 | 0.00191 | -0.0498 | 0.2077 | 0.9788 |
| 5.0 | 0.7920 | 0.00651 | 0.00222 | -0.0507 | 0.1630 | 0.9940 |
| 5.5 | 0.8597 | 0.00708 | 0.00257 | -0.0536 | 0.1219 | 0.9988 |
| 6.0 | 0.9143 | 0.00762 | 0.00293 | -0.0536 | 0.0911 | 1.0000 |
| 6.5 | 0.9624 | 0.00809 | 0.00328 | -0.0521 | 0.0703 | 1.0000 |
| 7.0 | 1.0124 | 0.00855 | 0.00366 | -0.0510 | 0.0552 | 1.0000 |
| 7.5 | 1.0634 | 0.00902 | 0.00405 | -0.0502 | 0.0447 | 1.0000 |
| 8.0 | 1.1144 | 0.00951 | 0.00447 | -0.0495 | 0.0366 | 1.0000 |
| 8.5 | 1.1652 | 0.01001 | 0.00492 | -0.0487 | 0.0306 | 1.0000 |
| 9.0 | 1.2159 | 0.01050 | 0.00538 | -0.0480 | 0.0266 | 1.0000 |
| 9.5 | 1.2660 | 0.01102 | 0.00587 | -0.0471 | 0.0232 | 1.0000 |
| 10.0 | 1.3151 | 0.01159 | 0.00642 | -0.0462 | 0.0203 | 1.0000 |
| 10.5 | 1.3633 | 0.01218 | 0.00699 | -0.0451 | 0.0182 | 1.0000 |
| 11.0 | 1.4109 | 0.01277 | 0.00760 | -0.0440 | 0.0166 | 1.0000 |
| 11.5 | 1.4565 | 0.01346 | 0.00827 | -0.0426 | 0.0150 | 1.0000 |
| 12.0 | 1.5011 | 0.01415 | 0.00898 | -0.0410 | 0.0138 | 1.0000 |
| 12.5 | 1.5442 | 0.01486 | 0.00971 | -0.0393 | 0.0130 | 1.0000 |
| 13.0 | 1.5828 | 0.01575 | 0.01062 | -0.0369 | 0.0118 | 1.0000 |
| 13.5 | 1.6169 | 0.01658 | 0.01149 | -0.0336 | 0.0113 | 1.0000 |
| 14.0 | 1.6490 | 0.01750 | 0.01245 | -0.0303 | 0.0108 | 1.0000 |
| 14.5 | 1.6780 | 0.01864 | 0.01364 | -0.0268 | 0.0102 | 1.0000 |
| 15.0 | 1.7027 | 0.02012 | 0.01516 | -0.0231 | 0.0094 | 1.0000 |

Table 8: XFOIL polars for NACA 2412 at $Re = 4 \cdot 10^6$: lift, drag, moment, and transition locations.

NACA 0012 data generated with XFOIL [15].

| $\alpha_{\text{deg}}$ | $C_L$ | $C_D$ | $C_{Dp}$ | $C_M$ | Top_Xtr | Bot_Xtr |
|---|---|---|---|---|---|---|
| -5.0 | -0.5553 | 0.00656 | 0.00199 | -0.0012 | 0.8985 | 0.0793 |
| -4.5 | -0.5007 | 0.00631 | 0.00174 | -0.0008 | 0.8662 | 0.0998 |
| -4.0 | -0.4460 | 0.00607 | 0.00152 | -0.0005 | 0.8288 | 0.1264 |
| -3.5 | -0.3911 | 0.00584 | 0.00131 | -0.0003 | 0.7880 | 0.1609 |
| -3.0 | -0.3357 | 0.00565 | 0.00115 | -0.0001 | 0.7438 | 0.1981 |
| -2.5 | -0.2802 | 0.00547 | 0.00100 | 0.0000 | 0.6992 | 0.2414 |
| -2.0 | -0.2245 | 0.00533 | 0.00089 | 0.0000 | 0.6541 | 0.2863 |
| -1.5 | -0.1686 | 0.00522 | 0.00080 | 0.0001 | 0.6069 | 0.3320 |
| -1.0 | -0.1124 | 0.00515 | 0.00074 | 0.0001 | 0.5610 | 0.3772 |
| -0.5 | -0.0562 | 0.00510 | 0.00070 | 0.0000 | 0.5159 | 0.4233 |
| 0.0 | 0.0000 | 0.00508 | 0.00069 | 0.0000 | 0.4705 | 0.4700 |
| 0.5 | 0.0562 | 0.00510 | 0.00071 | 0.0000 | 0.4236 | 0.5159 |
| 1.0 | 0.1124 | 0.00515 | 0.00074 | -0.0001 | 0.3772 | 0.5619 |
| 2.0 | 0.2245 | 0.00533 | 0.00089 | 0.0000 | 0.2856 | 0.6533 |
| 2.5 | 0.2802 | 0.00547 | 0.00100 | 0.0000 | 0.2412 | 0.6993 |
| 3.0 | 0.3357 | 0.00565 | 0.00115 | 0.0001 | 0.1982 | 0.7438 |
| 3.5 | 0.3911 | 0.00584 | 0.00131 | 0.0003 | 0.1613 | 0.7882 |
| 4.0 | 0.4460 | 0.00608 | 0.00152 | 0.0005 | 0.1263 | 0.8287 |
| 4.5 | 0.5008 | 0.00631 | 0.00174 | 0.0008 | 0.0999 | 0.8658 |
| 5.0 | 0.5553 | 0.00656 | 0.00199 | 0.0012 | 0.0795 | 0.8983 |
| 5.5 | 0.6095 | 0.00686 | 0.00226 | 0.0016 | 0.0623 | 0.9250 |
| 6.0 | 0.6628 | 0.00715 | 0.00255 | 0.0023 | 0.0514 | 0.9482 |
| 6.5 | 0.7156 | 0.00748 | 0.00285 | 0.0030 | 0.0428 | 0.9663 |
| 7.0 | 0.7689 | 0.00784 | 0.00318 | 0.0037 | 0.0361 | 0.9801 |
| 7.5 | 0.8266 | 0.00823 | 0.00353 | 0.0032 | 0.0308 | 0.9885 |
| 8.0 | 0.8854 | 0.00864 | 0.00391 | 0.0024 | 0.0269 | 0.9943 |
| 8.5 | 0.9492 | 0.00911 | 0.00434 | 0.0004 | 0.0234 | 0.9959 |
| 9.0 | 1.0117 | 0.00963 | 0.00482 | -0.0013 | 0.0203 | 0.9978 |
| 9.5 | 1.0738 | 0.01009 | 0.00528 | -0.0029 | 0.0189 | 0.9994 |
| 10.0 | 1.1260 | 0.01065 | 0.00582 | -0.0025 | 0.0167 | 1.0000 |
| 10.5 | 1.1706 | 0.01109 | 0.00627 | -0.0004 | 0.0159 | 1.0000 |
| 11.0 | 1.2158 | 0.01166 | 0.00684 | 0.0015 | 0.0147 | 1.0000 |
| 11.5 | 1.2626 | 0.01227 | 0.00747 | 0.0030 | 0.0136 | 1.0000 |
| 12.0 | 1.3108 | 0.01285 | 0.00806 | 0.0041 | 0.0131 | 1.0000 |
| 12.5 | 1.3578 | 0.01354 | 0.00876 | 0.0053 | 0.0122 | 1.0000 |
| 13.0 | 1.4027 | 0.01440 | 0.00965 | 0.0067 | 0.0111 | 1.0000 |
| 13.5 | 1.4488 | 0.01509 | 0.01038 | 0.0079 | 0.0109 | 1.0000 |
| 14.0 | 1.4930 | 0.01587 | 0.01120 | 0.0093 | 0.0105 | 1.0000 |
| 14.5 | 1.5347 | 0.01677 | 0.01214 | 0.0111 | 0.0100 | 1.0000 |
| 15.0 | 1.5726 | 0.01784 | 0.01325 | 0.0133 | 0.0094 | 1.0000 |

Table 9: XFOIL-generated polars for NACA 0012 at $Re = 4 \cdot 10^6$: lift, drag, moment, and transition locations.

# 4 Force Balance, Power & Energy Model

## 4.1 Aircraft Efficiencies

**Assumptions and Limitations:**

- The provided framework assumes fix system efficiencies. These can be changed as required for customized simulations.

| Item | Symbol | Value | Source |
|---|---|---|---|
| Electric Efficiency | $\eta_e$ | 0.9 | [16] |
| Hover Propulsive Efficiency | $\eta_{hp}$ | 0.7 | [17] |
| Propulsive Efficiency | $\eta_p$ | 0.85 | [16] |
| Hover System Efficiency | $\eta_h = \eta_e \cdot \eta_{hp}$ | 0.63 | [17] |
| Overall System Efficiency | $\eta_c = \eta_p \cdot \eta_e$ | 0.77 | [17] |

Table 10: System efficiencies.

## 4.2 Momentum Theory Power Model

**Assumptions and Limitations:**

- The power modelling within the provided framework is based on propeller momentum theory, using flight equilibrium relationships in hover, climb and cruise flight. For improved rotor dynamics accuracy, one should enhance this model using Blade Element Momentum Theory.
- Steady, unaccelerated flight (forces equilibrium) in each flight phase is assumed.
- For simulation, number of propeller in climb/cruise configuration is assumed to be 1. The number of vertical lift propeller is assumed to be 8.

### 4.2.1 Hover Power Required:

Power requirements in hover flight account for steady hover [18], where thrust and aircraft mass are balanced and power is needed to overcome propeller induced velocity, as illustrated in Fig. 4:

$$\sum F_z = 0 = T - W, \tag{34}$$

$$T_{required_{hover}} = MTOM \cdot g \tag{35}$$

resulting in a power requirement of:

$$P_{required_{hover}} = \frac{T_{total} \cdot v_i}{\eta_h} = \frac{MTOM \cdot g}{\eta_h} \cdot \sqrt{\frac{\sigma}{2 \cdot \rho}} \tag{36}$$

- $v_i$ $(m/s^2)$ = propeller induced velocity, defined by:

$$v_i = -\frac{V}{2} \cdot \sqrt{\left(\frac{V}{2}\right)^2 \cdot \frac{\sigma}{2\rho}} \tag{37}$$

- $\rho$ $(kg/m^2)$ = air density in hover.
- $\sigma$ $(N/m^2)$ = propeller disk loading, defined by:

$$\sigma = \frac{T_{prop}}{A_{prop}} = \frac{T_{prop}}{\pi \cdot R_{prop}^2} \tag{38}$$

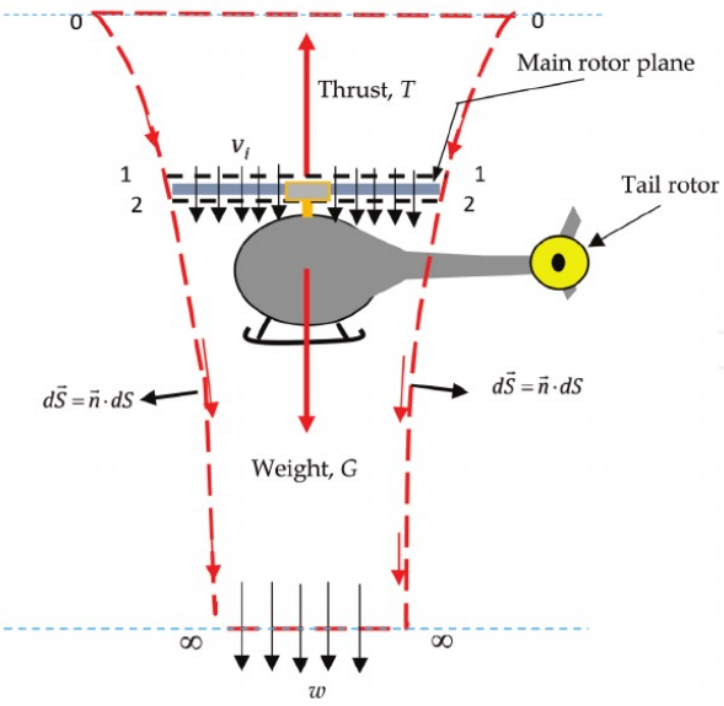


Figure 4: Forces in Hover, from Ref. [18].

#### 4.2.2 Climb Power Required:

The following calculations are based on the force balance equilibrium in steady climb flight [19] in the body frame, as illustrated in Fig. (5):

$$\sum F_x = 0 = T - D - W \cdot \sin(\theta), \tag{39}$$

$$\sum F_z = 0 = L - W \cdot \cos(\theta), \tag{40}$$

where $T$ is thrust (N), $D$ is drag (N), $W$ is aircraft weight (N), $L$ is lift (N), and $\theta$ is the climb angle.

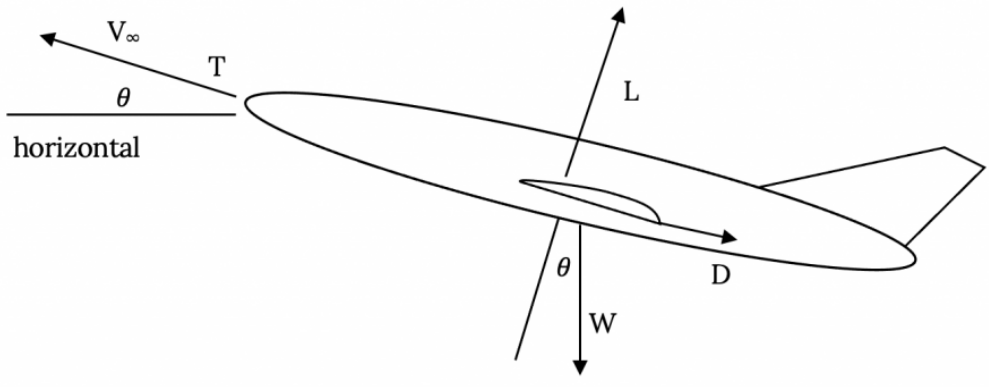


Figure 5: Forces in Climb, from Ref. [19].

The power required in climb is defined as:

$$P_{climb} = P_{req_{flight}} + P_{ind_{prop}} = \frac{T_{req_{climb}} \cdot V_{climb}}{\eta_c} + \frac{T_{prop_{climb}} \cdot v_i}{\eta_c} \cdot n_{prop} \tag{41}$$

- $P_{req_{flight}}$ (W) = power required to maintain flight, defined by:

$$P_{req_{flight}} = \frac{T_{req_{climb}} \cdot V_{climb}}{\eta_c} \tag{42}$$

- $T_{req_{climb}}$ (N) = thrust required in climb, illustrated in Fig. 5 and defined by:

$$T_{required_{climb}} = D_{climb} + MTOM \cdot g \cdot sin(\theta) \tag{43}$$

- $D_{climb}$ (N) = aircraft drag in climb flight (Eq. 33), using $V_{climb}$ (Eq. 47) and $\alpha_{climb}$.
- MTOM (kg) = max. take-off mass (Eq. 1).
- $\theta$ (°) = climb angle, assumed to be equal to angle of attack in climb $\alpha_{climb}$.
- $P_{ind_{porp}}$ (W) = propeller induced power required, defined by:

$$P_{ind_{prop}} = \frac{T_{prop_{climb}} \cdot v_i}{\eta_c} \cdot n_{prop} \tag{44}$$

- $T_{prop_{climb}}$ (N) = $T_{req_{climb}}/n_{prop}$ = thrust required per propeller.
- $n_{prop}$ (-) = number of propeller.
- $v_i$ (m/s) = propeller induced velocity, defined by Eq. 37

The horizontal speed during climb phase (Climb Speed), accounting for climb angle $\theta = \alpha_{climb}$, assuming zero wind, is defined by:

$$\text{Climb Condition: } MTOM \cdot g \cdot cos(\theta) = L = \frac{1}{2} \cdot \rho \cdot V_{climb}^2 \cdot S \cdot C_{L_{climb}} \tag{45}$$

Resulting in the trivial conditions during climb flight:

$$\text{Mass Condition: } MTOM = \frac{1}{2 \cdot g \cdot cos(\theta)} \cdot \rho \cdot V_{climb}^2 \cdot S \cdot C_{L_{climb}} \tag{46}$$

and,

$$\text{Climb Speed Condition: } V_{climb} = \sqrt{\frac{2 \cdot MTOM \cdot g \cdot cos(\theta)}{\rho \cdot S \cdot C_{L_{climb}}}}, \tag{47}$$

where $\theta$ is assumed to be equivalent to the angle of attack during climb $\alpha_{climb}$ (compare Section 3.2).

Due to the conceptual nature of our framework, moment balance is not explicitly modeled; however, we assume that the configuration is trimmed through appropriate tail or distributed propulsion arrangement.

#### 4.2.3 Cruise Power Required:

The following calculations are based on the force balance equilibrium in steady cruise [19] flight in the body frame, as illustrated in Figure 6:

$$\sum F_x = 0 = T \cdot \cos(\alpha_t) - D, \tag{48}$$

$$\sum F_z = 0 = L + T \cdot \sin(\alpha_t) - W, \tag{49}$$

where $T$ is thrust (N), $D$ is drag (N), $W$ is aircraft weight (N), $L$ is lift (N), and $\alpha_t$ is the thrust angle.

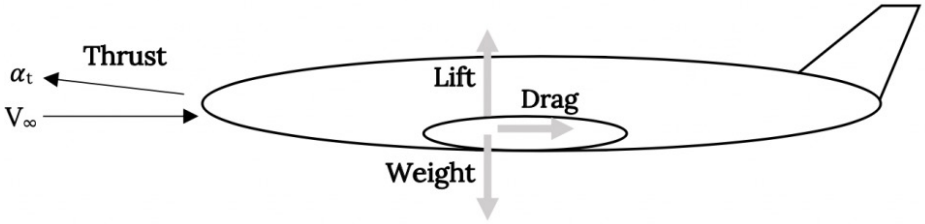


Figure 6: Static Force Balance in Straight and Level Flight, from Ref. [19].

The power required to maintain steady cruise flight is similar derived as cruise power, defined by:

$$P_{cruise} = P_{req_{flight}} + P_{ind_{prop}} = \frac{T_{req_{cruise}} \cdot V_{cruise}}{\eta_c} + \frac{T_{prop_{cruise}} \cdot v_i}{\eta_c} \cdot n_{prop} \tag{50}$$

- $T_{req_{cruise}}$ (N) = thrust required in cruise, illustrated in Fig. 6 and defined by:

$$T_{required_{cruise}} = \frac{D_{cruise}}{cos(\alpha_t)} = \frac{W - L}{sin(\alpha_t)} \tag{51}$$

- $D_{climb}$ (N) = aircraft drag in cruise flight (Eq. 33), using $V_{cruise}$ (Eq. 53)

During horizontal, unaccelerated flight, the cruise speed is derived by:

$$W = D \cdot \tan(\alpha_t) + L = \frac{\rho}{2} \cdot V_{\text{cruise}}^2 \cdot S \cdot (C_{D,\text{cruise}} \cdot \tan(\alpha_t) + C_{L,\text{cruise}}) \tag{52}$$

to get:

$$V_{cruise} = \sqrt{\frac{2 \cdot MTOM \cdot g}{\rho \cdot S \cdot (C_{D_{cruise}} \cdot tan(\alpha_t) + C_{L_{cruise}})}}, \tag{53}$$

where $\alpha_t$ is assumed to be equivalent to the angle of attack during cruise $\alpha_{cruise}$ (compare Section 3.2).

Due to the conceptual nature of our framework, moment balance is not explicitly modeled; however, we assume that the configuration is trimmed through appropriate tail or distributed propulsion arrangement.

### 4.3 Energy Requirements

The required energy (Wh) in each flight phase can be computed using the relationship:

$$E_i = \sum_i \text{P}_i \cdot t_i \tag{54}$$

The specific battery energy can be calculated when dividing the energy by battery mass:

$$e_i = \frac{E_i}{M_{bat}} \tag{55}$$

- $M_{bat}$ (kg) = battery mass, defined by Eq. 2, with:

$$E_{useable} = E_{trip} + E_{reserve} \tag{56}$$

- $E_{trip}$ (Wh) = sum of energy required in hover, climb and cruise, using Eq. 54.
- $E_{reserve}$ (Wh) = energy required in reserve flight, accounting for 30 min for VFR and 45min for IFR flight with cruise power according FAA.

Within this model the end-of-life battery status is considered, which is set to 80% of BOL (begin-of-life) capacity:

$$e_{BAT_{EOL}} = 0.8 \cdot \rho_{bat} \tag{57}$$

The battery ceiling is set as 90% SOC and the floor as 10% SOC, making these portions unusable for trips [17]. Resulting in usable specific energy:

$$e_{\text{usable}} = 0.8 \cdot e_{BAT_{EOL}} = 0.64 \cdot \rho_{bat} = e_{trip_{design}} + e_{reserve} \tag{58}$$

or expressed as the battery specific energy budget for the trip:

$$e_{trip_{design}} = 0.64 \cdot \rho_{bat} - e_{reserve} \tag{59}$$

or

$$e_{trip} \leq 0.64 \cdot \rho_{bat} - e_{reserve} \tag{60}$$

$$1.5623 \cdot (e_{trip} + e_{reserve}) \leq \rho_{bat} \tag{61}$$

Resulting in total battery energy storage capacity of:

$$E_{Bat_{total}} = \rho_{bat} \cdot M_{bat} \tag{62}$$

# 5 Economic Model

## 5.1 Operations Model

- The eVTOL operates within a daily operation window, defined by a fixed value of $T_D$ (hours).
- Within this operation window the eVTOL can perform flights, characterized by travel time $t_{trip}$ and battery depth-of-discharge (DOD), defined in Chapter 6.
- The time between each flight is defined as the turnaround-time $T_T$. This time accounts for battery recharging as well as passenger/freight swap, but within the model only battery recharging is considered.
- Time for battery recharge is defined by the charging rate $C_{rate_{charge}}$, defined in Chapter 6.

$$T_T = \frac{1}{C_{rate_{charge}}} \cdot DoD = \frac{1}{C_{rate_{charge}}} \cdot \frac{E_{trip}}{E_{Battery}} \tag{63}$$

with:

$$DoD = \frac{E_{trip}}{E_{Battery}} \tag{64}$$

The Total Cycle Time Factor (CT), measures the efficiency of transportation operations. It reflects the ratio of non-productive turnaround time to productive trip time, with the "+1" accounting for the complete cycle. A lower value indicates higher operational efficiency by minimizing turnaround time relative to trip time. It is defined by:

$$CT = \frac{T_T}{t_{trip}} + 1 \tag{65}$$

Fig. 7 depicts an operational framework for eVTOL vehicles, based on Uber Elevate requirements, Ref. [20]. It includes:

- **Annual Operation Days** ($n_{wd}$): 260 days/year.
- **Daily Operation Window** ($T_D$): 8 hours/day.
- **Turnaround Time** ($T_T$): Function of C-rate and Depth of Discharge (DoD).
- **Trip Time** ($T_{trip}$): Depends on vehicle speed (V), trip distance ($D_{trip}$), and hover time ($t_{hover}$).

The framework calculates the number of flight cycles and total flight hours within these constraints. Operational parameters like annual-trip-time ratio, annual flight hours, daily flight hours and flight cycles are defined below:

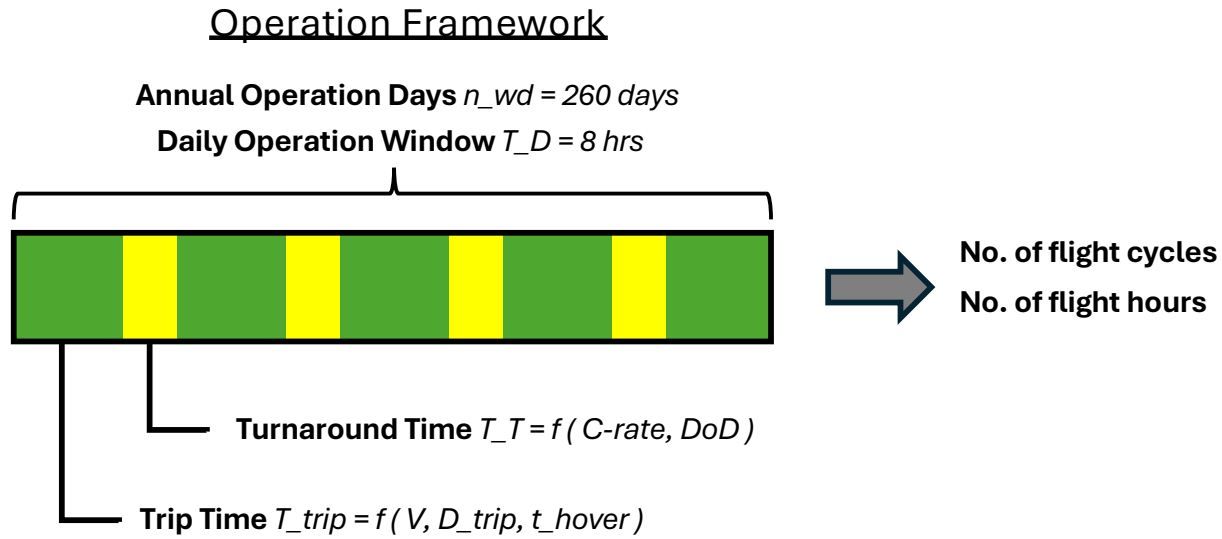


Figure 7: Operations Window.

- $\lambda_{trip}$ = **annual-trip-time ratio**, defined by Eq. 66 and 71:

$$\lambda_{trip} = \frac{t_{trip}}{FH_{annual}} \tag{66}$$

- $FH_{annual}$ (hours) = annual operating flight hours of one eVTOL, defined by Eq. 67 and 70:

$$FH_{annual} = t_{trip} \cdot FC_{annual} = t_{trip} \cdot n_{WD} \cdot FC_{day} \tag{67}$$

- $FC_{annual}$ (-) = annual operating flight cycles of one eVTOL, defined by:

$$FC_{annual} = n_{WD} \cdot FC_{day} = n_{WD} \cdot \frac{T_D}{t_{trip} \cdot CT} \tag{68}$$

- $n_{WD}$ (-) = number of operating days per year, set to 260, Ref. [17].
- $FC_{day}$ (-) = daily operating flight cycles of one eVTOL, defined by:

$$FC_{day} = \frac{T_D}{t_{trip} \cdot CT} \tag{69}$$

$$FH_{annual} = n_{WD} \cdot \frac{T_D}{CT} \tag{70}$$

and

$$\lambda_{trip} = \frac{1}{FC_{annual}} = \frac{t_{trip} \cdot CT}{n_{WD} \cdot T_D} \tag{71}$$

### 5.2 Operational Cost Model

**Assumptions and Limitations:**

- The total operating cost model is structured according the ATA-67 Formula for Direct Operating cost, Ref. [21].
- The sub-assumptions are based on highly variable operational assumptions in real world applications, which can be adjusted depending on the operational business.

#### 5.2.1 Total Operating Cost

The total operating costs of an aircraft per trip are divided into Cash Operating Cost (COC), Cost of Ownership (COO) and Indirect Operating Cost (IOC), according Ref. [21]:

$$TOC = COC + COO + IOC \tag{72}$$

Each cost element is further subdivided into its components, as shown in Figure 8, in order to obtain as detailed a picture as possible of the cost structure of an eVTOL. The cost calculation is based on the fact that the flight hour is the only value-adding activity of an operator. Therefore, all costs associated with flight operations must be allocated to the flight hour. The sum of COC and COO is also regarded as Direct Operating Cost (DOC), similar to variable costs, and IOC as fixed costs.

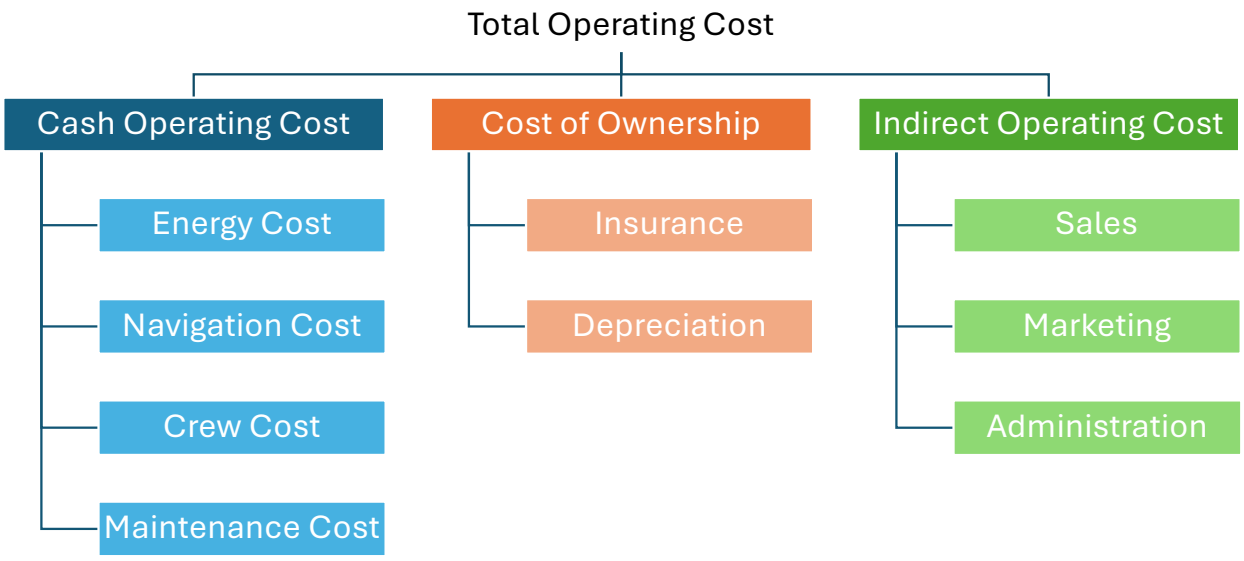


Figure 8: Total operating cost structure.

### 5.2.2 Cash Operating Cost

Cash operating costs in aviation, akin to variable costs, encompass immediate, out-of-pocket expenses. In this model, they are considered on a trip base and include energy cost $C_E$, maintenance cost $C_M$, crew cost $C_C$, and navigation cost $C_N$:

$$COO = C_E + C_M + C_C + C_N \tag{73}$$

**Energy Cost**

**Assumptions and Limitations:**

- The framework assumes the energy price and electricity $CO_2$ emissions of Germany, accounting 0.096 €/kWh and 0.3784 kg-$CO_2$/kWh respectively.
- A dataset for energy prices and $CO_2$ emissions is provided on the authors GitHub and can be used for geographic specific analysis.

Energy cost, comparable to fuel cost of combustion-engine aircraft, are defined by the simple relationship:

$$C_E = E_{trip} \cdot P_{energy} \tag{74}$$

with trip energy $E_{trip}$ (kWh) and current energy price $P_{energy}$ (€/kWh). $E_{trip}$ is the used energy amount of the trip flown, and is direct related to power requirements in each flight phase and flight time, thus to mission profile design (velocity, altitude etc.). It is considered, that $P_{energy}$ can vary depending on procedures for generation of electricity, differing in geographical regions, countries and energy policy.

**Maintenance Cost**

**Assumptions and Limitations:**

- The computation of this model is based on several static operational assumptions that can significantly influence the potential result.
- $t_{trip}$ in this section is considered in hours.

The maintenance costs, $C_M$, are defined by:

$$C_M = C_{M_{WR}} + C_{M_B} \tag{75}$$

with $C_{M_{WR}}$ are the **wrap-rated maintenance costs**:

$$C_{M_{WR}} = MF \cdot MWR \cdot t_{trip} = 0.6 \cdot 55 \cdot t_{trip} = 33 \cdot t_{trip} \tag{76}$$

- MF (-) = maintenance man-hours per flight hour ratio, assumed as 0.6, Ref. [16].
- MWR (€/hr) = maintenance wrap-rate, assumed fix at 55€, Ref. [16].
- $t_{trip}$ (hr) = trip duration of the considered flight.

$C_{M_B}$ is considered as **battery replacement cost**, defined by:

$$C_{M_B} = n_{Bat} \cdot P_{Bat_s} \cdot E_{BAT_{total}} \cdot \lambda_{trip} \tag{77}$$

- $E_{BAT_{total}}$ (kWh) = **total energy storage capacity** of the eVTOL installed battery, defined by Eq. 62 in Chapter 4.3.
- $P_{bat_s}$ (€/kWh) = **energy specific battery acquisition cost**. According to [22], the Tesla Model S battery cost was estimated at 155 €/kWh in 2020 and 55 €/kWh in 2030, with current costs ranging from 108 €/kWh to 142 €/kWh. Future eVTOL batteries will likely have higher capacities, requiring special attention, as battery costs can significantly impact the total cost.

**Assumptions and Limitations:**

- The following trivial assumption applies: Traveling a design trip distance corresponds to discharging one battery charge. In other words, the battery of the eVTOL is designed in such a way that it is sufficient to cover the design trip distance, after which it must be recharged to cover the same distance again. The discharge in the design trip distance does not mean a complete battery discharge, as unusable energy and reserves are also taken into account.
- It is assumed that the reserve is not used, but is considered as energy reserve in battery design.
- When considering the cycle life of the battery, it is assumed that the eVTOL flies the design distance on every flight.

- $n_{Bat}$ (-) = **number of required batteries per year**. This is highly dependent on the specific battery characteristics and discharge rates. A model for battery cycle-life is proposed and derived in the following:

$$n_{Bat} = \frac{CC_{req_{eVTOL}}}{N_{cycles}} \tag{78}$$

- $CC_{req_{eVTOL}}$ (-) = **annually required charging cycles** of the eVTOL, defined by:

$$CC_{req} = \frac{FC_{annual}}{FC_{Bat}} = n_{WD} \cdot \frac{T_D}{t_{trip} \cdot DH} \cdot \frac{SE_{trip}}{SE_{trip_{design}}} \tag{79}$$

- $FC_{Bat}$ (-) = number of flight cycles that can be flown with one battery charge, corresponds to the ratio of design trip specific energy available $SE_{trip_{design}}$ to flown trip energy $SE_{trip}$, where $SE_{trip_{design}}$ is defined by Eq. 59 in Chapter 4.3:

$$FC_{Bat} = \frac{SE_{trip_{design}}}{SE_{trip}} = \frac{E_{trip_{design}}}{E_{trip}} \tag{80}$$

**Assumptions and Limitations:**

- The charge cycle amount of Li-Ion batteries for EV applications is dependent on the allowed end-of-life losses, set to $20\%$ (equals $80\%$ of begin-of-life battery capacity), and average discharge rate ($C_{rate}$).

- Within the provided framework we establish an empirical model to estimate the battery cycle life according Eq. 102.
- As alternate approach, one can consider a constant charging loss rate $Loss_{charge}$ of $0.048\%$ according Ref. [22].
- $N_{cycles}$ (-) = **number of life cycles available per battery**, based on the average C-rate $C_{rate_{vaerage}}$, depth-of-discharge (DoD) and chraging rate, until $20\%$ degradation relative to begin-of-life (BOL) condition is met. $CC_{avlb_{Bat}}$ is determined empirical within this framework, based on Eq. 102 in Chapter 4.3.

$$n_{bat_{req}} = \frac{1}{N_{cycles}} \cdot \frac{n_{WD} \cdot T_D}{t_{trip} \cdot DH} \cdot \frac{e_{\text{trip}}}{e_{\text{tripm}}} \tag{81}$$

- Substituting Eq. 71 and Eq. 81 in Eq. 77 yields the battery replacement cost function, delivering €/trip:

$$C_{M_B} = \frac{1}{N_{cycles}} \cdot P_{Bat_s} \cdot E_{BAT_{total}} \cdot \frac{e_{\text{trip}}}{e_{\text{tripm}}} \tag{82}$$

**Navigation Cost**

**Assumptions and Limitations:**

- The framework proposes two navigation cost computation methods, both based on german air traffic control charge authority (DFS), Ref. [23].
- The proposed simulation uses Method 1 with Eq. 83 to map the navigation fees as accurately as possible.
- Eq. 86 is proposed to use to count for uncertainties in airport charges, as they can differ dependent on aircraft characteristics, averaging the navigation fees for all eVTOL aircraft and making them soley trip distance dependent.

**Method 1:** In this model the navigation charges for terminal services $C_{TS}$ and en-route services $C_{ER}$ of DFS (Deutsche Flugsicherung; german air traffic management agency) [23] are considered.

$$C_N = C_{TS} + C_{ER} \tag{83}$$

with

$$C_{TS} = \left(\frac{MTOM}{1000 \cdot 50}\right)^{0.7} \cdot unitrate \tag{84}$$

and

$$C_{ER} = \left(\frac{MTOM}{1000 \cdot 50}\right)^{0.5} \cdot \frac{D_{trip}}{100} \cdot unitrate \tag{85}$$

**Method 2:** Actually, there will be additional airport specific landing and take-off charges in real-world operation. As these can differ significantly depending on region of operation, the DFS charges can be considered for the maximum MTOM certifiable of 5.700kg according EASA SC-VTOL Ref. [1] and a unit rate of 80.14€ (2024) [23] to simplify the model, resulting in total navigation charges for one trip:

$$C_N = 17.526 + 0.2706 \cdot D_{trip} \tag{86}$$

**Crew Cost**

**Assumptions and Limitations:**

- There are two proposed crew cost model methods. Method 1 in Eq. 88 is used within the demonstrated analysis.
- Method2, Eq. 90, is more simplified and not accounts for bunker based pilots.

**Method 1:** The crew cost per trip is defined by:

$$C_C = C_{Crew} + C_{Cabin} \tag{87}$$

Due to the predicted nature of operation for eVTOL, no cabin crew will be considered in this model, reducing Eq. 87 to:

$$C_C = C_{Crew} = S_P \cdot n_{pilot} \cdot \lambda_{trip} = S_P \cdot \frac{t_{trip} \cdot CT}{U_{pilot} \cdot n_{AC}} \tag{88}$$

- $S_P$ (€/year) = annually eVTOL pilot salary. A helicopter pilot salary of 80.850€ per year in 2024 in Germany is assumed, Ref. [24].
- $\lambda_{trip}$ (-) = annual trip time ratio, as defined by Eq. 66 and 71.
- $n_{pilot}$ (-) = number of pilots needed to operate the eVTOL over the year.

$$n_{pilot} = n_{WD} \cdot \frac{T_D}{U_{pilot} \cdot n_{AC}} \tag{89}$$

- $U_{pilot}$ (hrs) = annually utilization of one pilot, assuming 2.000 hours per pilot per year.
- $n_{AC}$ (-) = number of aircraft controlled by one pilot/operator. For pilot on-board assume $n_{AC} = 1$. For bunker-based pilot operation assume $n_{AC}$ up to 8.

**Method 2:** An alternate and simplified model for crew cost would assume as fixed hourly salary of 39€ [24], resulting in:

$$C_{Crew} = 39 \cdot \frac{t_{trip}}{N_{AC}} \tag{90}$$

### 5.2.3 Cost of Ownership

**Assumptions and Limitations:**

- Accounting for costs of annual depreciation and aircraft insurance, distributed on the flight hour.
- Annual depreciation directly depends on eVTOL acquisition cost. The eVTOL acquisition cost is derived using the empty mass specific price, Ref. [17].
- The estimated values can differ from real world negotiated aircraft purchase prices. Further research is required at a time more data on eVTOL prices is available.
- For the annuity, fixed financial assumptions are made.

This model covers the cost of ownership in aircraft, considering depreciation $C_{dep}$ and insurance $C_{ins}$, including the financial loss from the aircraft's decreasing value over time and the regular payments for coverage against potential damages or liabilities:

$$COO = C_{dep} + C_{ins} = j \cdot P_{S_{empty}} \cdot M_{empty} \cdot \frac{t_{trip} \cdot CT}{n_{WD} \cdot T_D} + x_{ins} \cdot COC \tag{91}$$

- $C_{dep}$ (€) = **depreciation cost**, defined by:

$$C_{dep} = DEP_a \cdot \lambda_{trip} = DEP_a \cdot \frac{t_{trip} \cdot CT}{n_{WD} \cdot T_D} = j \cdot P_{S_{empty}} \cdot M_{empty} \cdot \frac{t_{trip} \cdot CT}{n_{WD} \cdot T_D} \tag{92}$$

where $DEP_a$ is the annual depreciation costs [25], defined by:

$$DEP_a = TDA \cdot \frac{i \cdot (1 - RV) \cdot (1 + i)^n}{(1 + i)^n - 1} = j \cdot TDA = j \cdot P_{S_{empty}} \cdot M_{empty} \tag{93}$$

- TDA (€) = $P_{S_{empty}} \cdot M_{empty}$ = total depreciation amount, assumed to be equal to the acquisition price of an eVTOL. According [26], considering a cummulative order value of €7.4bn for 2.770 vehicles of EVE Air Mobility eVTOL's, the average investment was €2.8m. In this model we assume a relationship between the empty weight $M_{empty}$ and eVTOL acquisition costs in line with Ref. [17], with an specific cost factor of $P_{s_{empty}}$=1.436,5 €/$kg_{empty}$ per kg empty weight.
- $j$ (-) = annuity factor. Annual fraction of the total depreciation amount (TDA). Considering the made assumptions, this is set within the model for $j = 0.0796$.
- i (%) = interest rate percentage, set to 3%.
- RV (%) = percentage residual value of investment, set to 5%.
- n (years) = annuity number of years, set to 15 years.
- $C_{ins}$ (€) = **insurance cost**, defined by:

$$C_{ins} = x_{ins} \cdot COC \tag{94}$$

- $x_{ins}$ (%) = insurance factor. Assumed to be fix at 6%, Ref.[22].

**Assumptions and Limitations:**

- Within the provided simulation, follwing is assumed:
- $j = 0.0796$
- $x_{ins} = 0.06$
- $P_{S_{empty}}$ = 1.436,5 €/kg
- Resulting in a cost of ownership model of:

$$COO = C_{dep} + C_{ins} = 114.345 \cdot M_{empty} \cdot t_{trip} \cdot 4.61538 \cdot 10^{-4} + 0.06 \cdot COC \tag{95}$$

### 5.2.4 Indirect Operating Cost

Indirect operating costs for aircraft include expenses such as reservation and sales expenses, advertising and publicity, and general and administrative costs, which are necessary for the overall support and management of aviation operations but not directly tied to flight activities. In this model it is assumed, that these costs can be derived as fraction of the DOC [27]:

$$IOC = C_{I_{RS}} + C_{I_{AP}} + C_{I_{GA}} = (x_{IRS} + x_{IAP} + x_{IGA}) \cdot DOC \tag{96}$$

- $DOC$ (€) = $COC + COO$ = direct operating cost, sum of cash operating cost (COO) and cost of ownership (COO).
- $C_{I_{RS}}$ (€) = reservation and sales expanses (14% of DOC)
  - $x_{IRS}$ (%) = reservation & sales factor.
- $C_{I_{AP}}$ (€) = advertising and publicity costs (2% of DOC)
  - $x_{IAP}$ (%) = advertising & publicity factor.
- $C_{i_{GA}}$ (€) = general and administrative costs (6% of DOC)
  - $x_{IGA}$ (%) = general & administration factor.

**Assumptions and Limitations:**

- The provided framework assumes the following, Ref. [27]:
- $x_{IRS}$ = 14%
- $x_{IAP}$ =2%
- $x_{IGA}$ = 6 %

$$COO = (0.14 + 0.02 + 0.06) \cdot DOC = 0.22 \cdot (COC + COO) \tag{97}$$

**Sepcific Cost** Using specific total operating costs, so TOC per trip divided by kilometers and seats (Eq. 98) or adjusted by load factor, the passenger-specific operating costs (Eq. 99), allows for a more precise comparison of cost efficiency across different routes and aircraft, reflecting both operational and market performance.

$$TOC_s = \frac{COC + COO + IOC}{N_s \cdot D_{trip}} = \frac{TOC}{N_s \cdot D_{trip}}(eur/skm) \tag{98}$$

$$TOC_sp = \frac{COC + COO + IOC}{N_s \cdot LF \cdot D_{trip}} = \frac{TOC}{N_s \cdot LF \cdot D_{trip}}(eur/skm) \tag{99}$$

- $N_s$ is the number of seats of the aircraft
- LF is the load factor during the journey

Taking Eq. 99 per trip we can consider this as the break-even ticket price for one seat for one trip, which a flight operator must charge in order to avoid losses:

$$TOC_{P_{trip}} = \frac{TOC}{N_s \cdot LF}(eur) \tag{100}$$

### 5.3 Revenue and Profitability Model

The eVTOL revenue and profit model is designed to simulate the profitability and economic incentives for future eVTOL operators. The revenue ($Rev$) generated from a single flight is calculated as the product of the trip distance ($d_{\text{trip}}$) and a fixed trip rate ($fare$) based on London ground taxi services, Ref. [28], assumed to be £1.70, which is approximately €1.98 as of August 2024.:

$$Rev = fare \cdot d_{\text{trip}}$$

The profit from each flight ($Profit_{\text{flight}}$) is then computed by subtracting the total operating cost ($TOC$) from the revenue:

$$Profit_{\text{flight}} = Rev - TOC$$

To determine the annual profit ($Profit_{\text{annual}}$), the profit per flight is multiplied by the annual number of flight cycles ($FC_{\text{annual}}$):

$$Profit_{\text{annual}} = (Rev - TOC) \cdot FC_{\text{annual}}$$

This model enables the assessment of the financial viability of eVTOL operations by evaluating revenue potential and operational costs across different trip scenarios.

The author is aware that the real-world revenue for an eVTOL trip would include an additional VAT, as in Germany approx. 19% VAT. However, as this may vary by region, it is not taken into account in this model.

## 6 Battery Degradation Model

**Assumptions and Limitations:**

- Within the provided framework, two methods are proposed to account for degrading battery energy storage capacity over operation time.

- **Method 1** encounters an self-developed empirical model to connect battery cycle life with depth-of-discharge (DoD), and C-rate during charge and discharge. This method is used within the provided simulations.
- **Method 2** is derived using a fixed degradation [22] factor at 1C discharge rate and is not accounting for DoD and charging rate.
- It must be mentioned that the simulation results of the battery consumption (numbers of the batteries) depend very much on the battery degradation model used. A reasonable enhancement of the model could be the integration of a more accurate and efficient battery degradation model in future work.

### 6.1 Method 1: Empirical Model

This section provides a brief overview of the empirical model developed to estimate the cycle life of a battery as a function of Depth of Discharge (DoD), charging C-rate, and discharging C-rate. The model is based on data DoD and cycle-life data of Ref. [29] and [30], interpolated for accuracy, and adjusted for harsh environmental conditions such as those encountered in eVTOL operations.

**Assumptions and Limitations:**

- **Data Adjustment**: The provided cycle life data was reduced by a factor of 4 to simulate the more extreme conditions expected in eVTOL applications and account for degradation down to 80% of begin-of-life (BOL) capacity.
- **Interpolation**: A piecewise linear interpolation was used to fit the DoD data. This approach ensures that the model captures the observed trend accurately.The data was segmented at DoD = 0.8. Separate linear fits were applied to the segments below and above this threshold.
- **Empirical Formula**: The provided model incorporates the effects of DoD, charging C-rate, and discharging C-rate, as a result of interpolation and estimation. Further research required to capture more accurate models for battery degradation of eVTOL.

The empirical model for cycle life $N_{\text{cycles}}$ as function of DoD is illustrated in Fig. 9 and defined as:

$$N_{\text{cycles}}(\text{DoD}) = \begin{cases} a_1 \cdot \text{DoD} + b_1, & \text{for DoD} \leq 0.8 \\ a_2 \cdot \text{DoD} + b_2, & \text{for DoD} > 0.8 \end{cases}$$

- The ‘pchip‘ (Piecewise Cubic Hermite Interpolating Polynomial) method is used for smooth interpolation of the given data points, and basic linear fitting (‘polyfit‘) is applied to derive the segmented linear model.

In this model, a DoD over 80% is avoided according to Ref. [17], therefore the model is reduced to:

$$N_{cycles}(\text{DoD}) = a_1 \cdot DoD + b_1 \tag{101}$$

This is further adjusted by the following, assuming that the charge rates are linked to the cycles via a power ratio:

$$N_{\text{cycles}} = N_{\text{cycles}}(\text{DoD}) \cdot \left( \frac{1}{\text{C-rate}_{\text{discharge}}^{c}} \right) \cdot \left( \frac{0.5}{\text{C-rate}_{\text{charge}}^{d}} \right)$$

Where:

- $a_1, b_1, a_2, b_2$ are the fitted parameters for the piecewise linear segments.
- $c = 1.1$ and $d = 1.2$ are empirically estimated coefficients that account for the effects of discharging and charging rates, respectively.

- **Fitted Parameters**:

$$\text{For DoD} \leq 0.8 : a_1 = -5986.8421, b_1 = 11776.3158$$
$$\text{For DoD} > 0.8 : a_2 = -20793.2692, b_2 = 20769.2307$$

This results in the follwing used equation:

$$N_{\text{cycles}} = (-5986.8421 \cdot DoD + 11776.3158) \cdot \left( \frac{1}{\text{C-rate}_{\text{discharge}}^{1.1}} \right) \cdot \left( \frac{0.5}{\text{C-rate}_{\text{charge}}^{1.2}} \right) \tag{102}$$

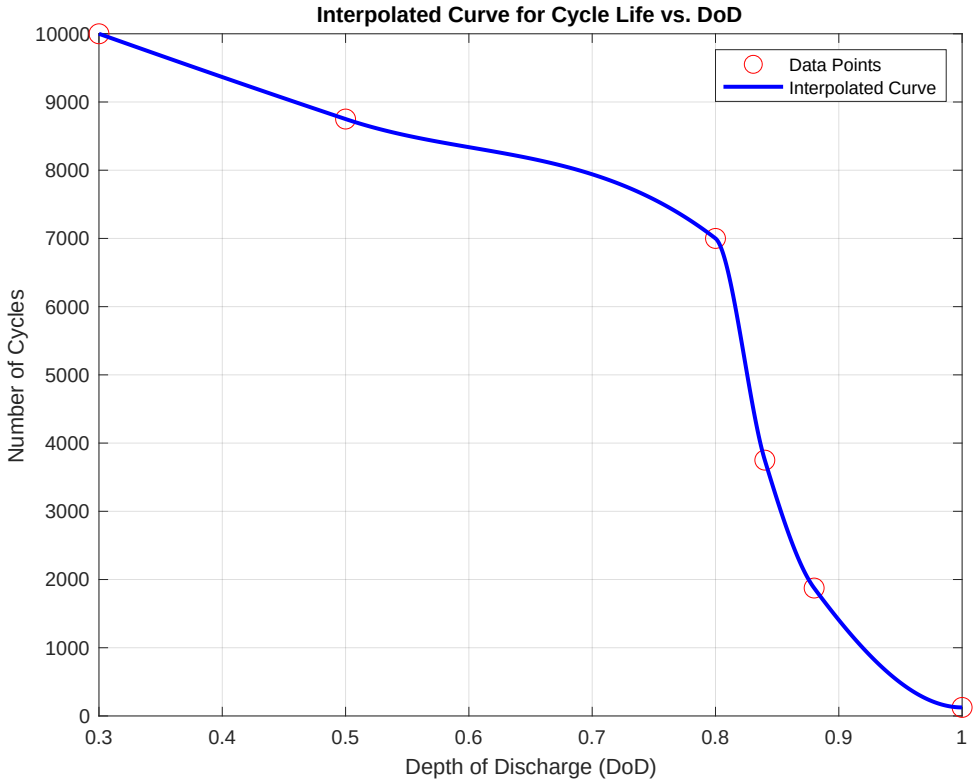


Figure 9: Interpolated Curve for Cycle Life vs. DoD

With:

- **Discharge Rate:** $C - rate_{discharge} = \frac{C_{\text{rate\_hover}} \cdot t_{\text{hover}} + C_{\text{rate\_climb}} \cdot t_{\text{cl}} + C_{\text{rate\_cruise}} \cdot t_{\text{cr}}}{t_{\text{tot}}}$: Average C-rate across the different phases of flight.
- $C_{\text{rate\_hover}} = \frac{\text{Power}_{\text{hover}}}{E_{\text{battery}}}$: C-rate during hover, defined as the ratio of hover power to total battery energy.
- $C_{\text{rate\_climb}} = \frac{\text{Power}_{\text{climb}}}{E_{\text{battery}}}$: C-rate during climb, defined as the ratio of climb power to total battery energy.
- $C_{\text{rate\_cruise}} = \frac{\text{Power}_{\text{cruise}}}{E_{\text{battery}}}$: C-rate during cruise, defined as the ratio of cruise power to total battery energy.
- $E_{\text{battery}} = \rho_{\text{bat}} \cdot m_{\text{bat}}$: Total energy capacity of the battery in Wh.
- **Charge Rate:** $C - rate_{charge}$ is assumed to be a design variable within the framework, so set fixed and changed as required.
- **DoD:** $DOD = \frac{E_{trip}}{E_{Battery}}$, ratio of energy used to total stored energy.

The resultant battery cycle-life envelope is illustrated in Fig. 10 for a constant $C - rate_{charge}$ of 2C. The empirical model developed provides a first estimation of battery cycle life across different DoD and C-rate conditions, based on battery data. The piecewise linear approach effectively captures the sharp decrease in cycle life observed at higher DoD levels.

### 6.2 Method 2: Static Degradation

**Assumptions and Limitations:**

- This method delivers a simpler and static approach for battery cycle-life estimation, making the model less dynamic.

From Ref. [22] the average degradation of the battery per charging cycle is $Q_{cycle} = 0.048\%$. Assuming an allowed degradation of $D = 20\%$, the number of life cycles for the eVTOL is:

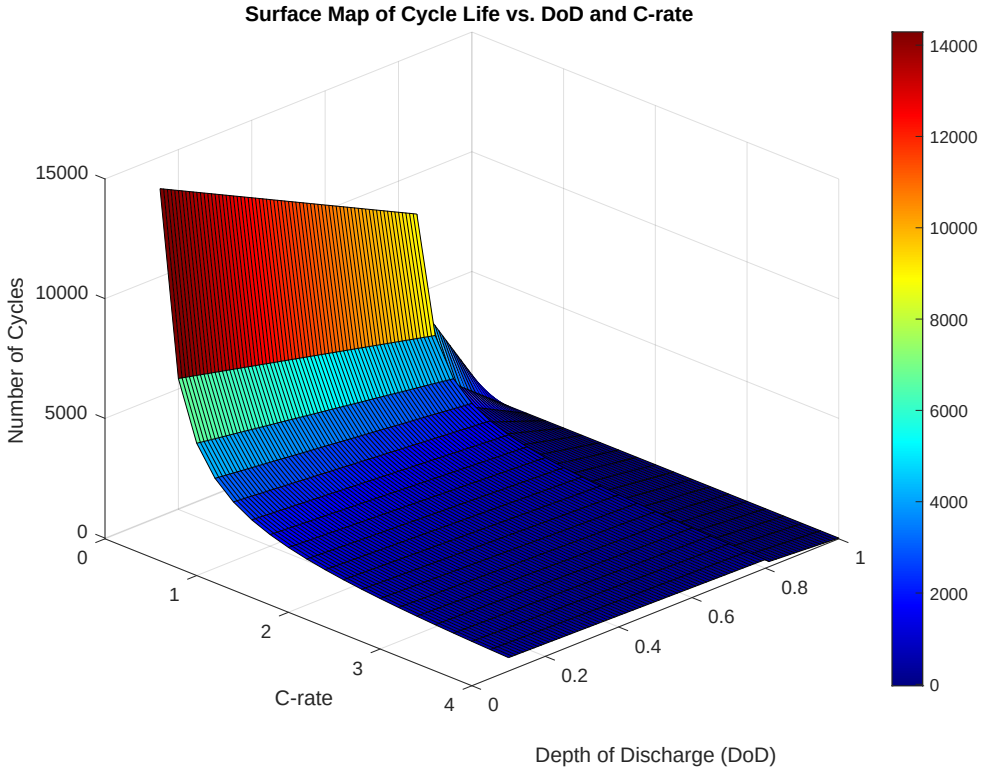


Figure 10: Piecewise Linear Fit for Cycle Life vs. DoD

$$N_{cycles} = \frac{D}{Q} = \frac{20}{0.048} = 416.67 \tag{103}$$

# 7 Constraint Model

## 7.1 Rotor Noise Modeling

This section provides supporting information on the acoustic modeling of eVTOL rotor systems used in the optimization. It includes both tonal and broadband noise models, used to estimate Sound Pressure Levels (SPL) during hover, climb, and cruise. All values are referenced to standard atmospheric conditions at mean sea level (MSL) and ambient temperature $T = 288.15\,\mathrm{K}$.

### 7.1.1 Tonal Noise in Hover: Gutin–Deming Model

Tonal rotor noise during hover is modeled using the Gutin–Deming formulation:

$$p_{\text{rms}}(\Omega, r, T, Q, \vartheta) = \frac{qn\Omega}{2\sqrt{2\pi}cr} \left| -T\cos\vartheta + Q\frac{c}{\Omega R_e^2} \right| J_{qn}(kR_e \sin\vartheta) \tag{104}$$

$$k = \frac{qn\Omega}{c} \tag{105}$$

$$SPL_{\text{rotor}} = 20\log_{10}\left(\frac{p_{\text{rms}}}{p_0}\right), \quad SPL_{\text{total}} = SPL_{\text{rotor}} + 10\log_{10}(n_{\text{rotor}}) \tag{106}$$

**Where:**

- $\Omega$: rotor angular velocity [rad/s]
- $r$: observer distance [m], set to 76.2 m (250 ft)
- $T$: rotor thrust [N], $Q$: torque [Nm]
- $c$: speed of sound [m/s]
- $R_e = 0.8R_t$: effective rotor radius [m]
- $q$: harmonic index, set to 1
- $n$: blade count, set to 2
- $\vartheta$: observer angle from rotor axis [rad]
- $J_{qn}$: Bessel function of the first kind
- $p_0 = 2 \cdot 10^{-5}$ Pa: reference pressure

The total sound pressure level for all rotors $SPL_{\text{total, hover}}$ is defined in Eq. (106), where $SPL_{\text{rotor, hover}}$ is the SPL of a single rotor, and $n_{\text{rotor,hover}}$ is the number of rotors for vertical lift. This expression assumes incoherent addition of sound power from multiple independent rotors running at the same speed [20].

A heatmap illustrating $SPL_{\text{total}}$ as a function of observer distance and hover rotor radius is provided in Fig. 11.

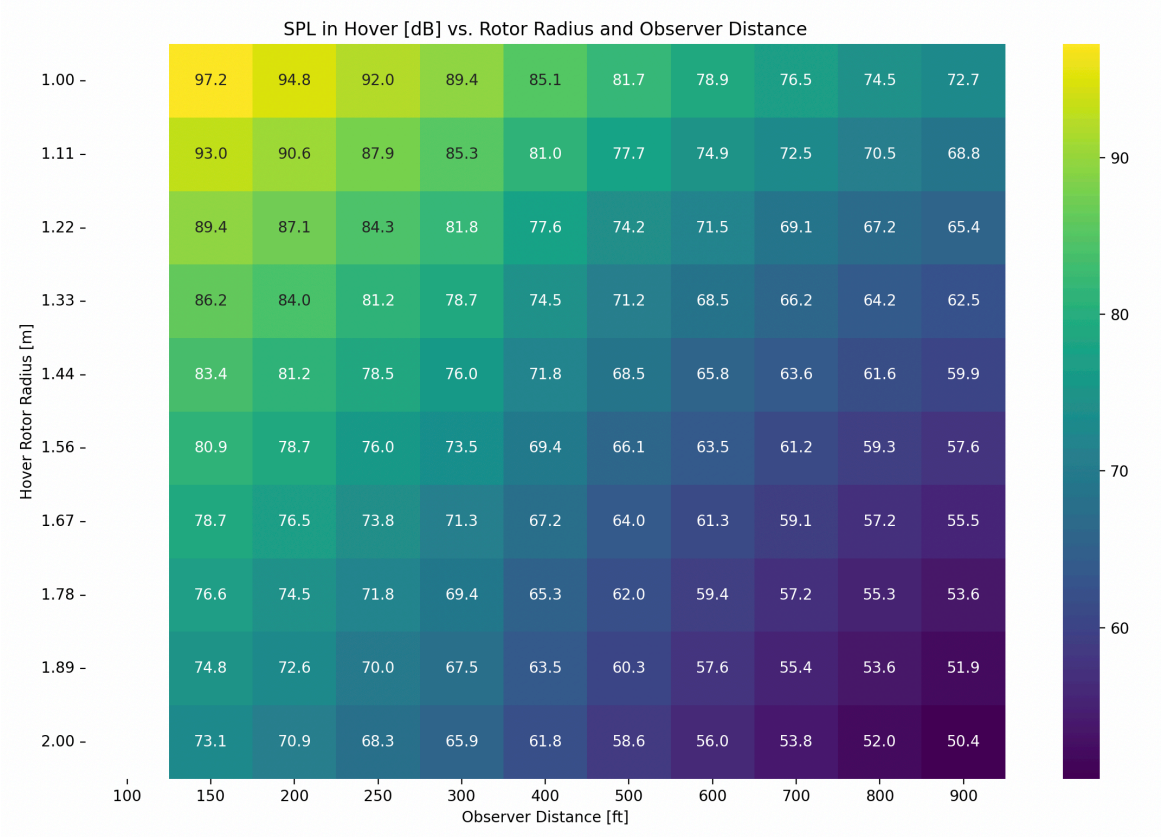


Figure 11: Hover SPL [dB(A)] from the Gutin–Deming model as a function of rotor radius and observer distance.

### 7.1.2 Broadband Noise: SKM Model

The broadband SPL in forward flight is estimated using the Schlegel–King–Mull (SKM) semi-empirical model [31]:

$$SPL_{\text{BB}} = 10\log_{10}\left(\frac{K\,A_{\text{prop}}\,V_{0.7}^{6}}{P_{\text{ref}}^{2}}\right) + 20\log_{10}\left(\frac{C_L}{C_{L,\text{ref}}}\right) + 20\log_{10}\left(\frac{300}{h_{\text{obs,ft}}}\right) \tag{107}$$

**Where:**

- $A_{\text{prop}}$: propeller disk area [$\text{m}^2$]
- $V_{0.7}$: blade tip speed at 70% radius [m/s]
- $C_L$: lift coefficient of propeller
- $K = 6.1 \times 10^{-27}$, $P_{\text{ref}}^2 = 10^{-16}\,\text{Pa}^2$
- $C_{L,\text{ref}} = 0.4$, $h_{\text{obs,ft}}$: observer altitude [ft]

### 7.1.3 Assumptions Summary

Table 11: Key acoustic model assumptions

| **Parameter** | **Assumed Value / Note** |
|---|---|
| Thrust coefficient $C_T$ | 0.1 (urban hover assumption, [32]) |
| Rotor count (hover) $n_{\text{rotor}}$ | 8 (lift+cruise) |
| Observer distance (hover) $r$ | 250 ft (76.2 m) |
| Observer angle $\vartheta$ | $\theta = \pi/2 + arcsin(h_{hover_{ft}}/r_{obs_{ft}})$ |
| Speed of sound $c$ | 340.3 m/s (MSL) |
| Ambient conditions | ISA, $T = 288.15\,\text{K}$, $\rho = 1.225\,\text{kg/m}^3$ |

### 7.1.4 Limitations

The models are suitable for conceptual design and trade-off studies but do not capture: (i) interaction noise effects, (ii) unsteady loading and vortex shedding, (iii) cumulative urban exposure (e.g., DNL), and (iv) psychoacoustic perception. These effects should be addressed using higher-fidelity simulations in future design stages.

## 7.2 Wing-Rotor Geometry Constraint

The lifting rotor radius tends to reach the upper limit during optimization design because a lower disk loading reduces power consumption [11]. A geometry constraint is implemented to prevent interferences between the lifting rotors, their attachment to the wings and minimum distances between the lifting rotors and between the lifting rotors and the fuselage ($d$), where the fuselage width is $w$. $d$ is set fix to 0.0125m, as required by EASA, Ref. [7]. This condition applies to both the rotor radii $R_{prop_{hover}}$ and the span $b$. Eq. 108 and 109 are based on an lift plus cruise condition with 8 lifting rotors, as used in the demonstrated framework. Eq. 110 illustrates this approach for an undefined number of lifting rotors, but only considers $n_{lifter} \geq 4$ and $n_{lifter} \in 4\mathbb{Z}$ Fig. 12 illustrates this restriction.

$$\text{Wingspan Condition: } \frac{b}{2} \geq (3 \cdot R_{prop_{hover}} + 2 \cdot d + \frac{w}{2}) \tag{108}$$

resulting in minimum wing span $b_{min}$,

$$b_{min} = 2 \cdot (3 \cdot R_{prop_{hover}} + 2 \cdot d + \frac{w}{2}) \tag{109}$$

or for undefined number of rotors:

$$b_{min} = 2 \cdot \left( \left( \frac{1}{4} \cdot n_{lifter} \cdot 2 \cdot R_{prop_{hover}} - R_{prop_{hover}} \right) + \frac{1}{4} \cdot n_{lifter} \cdot d + \frac{w}{2} \right) \tag{110}$$

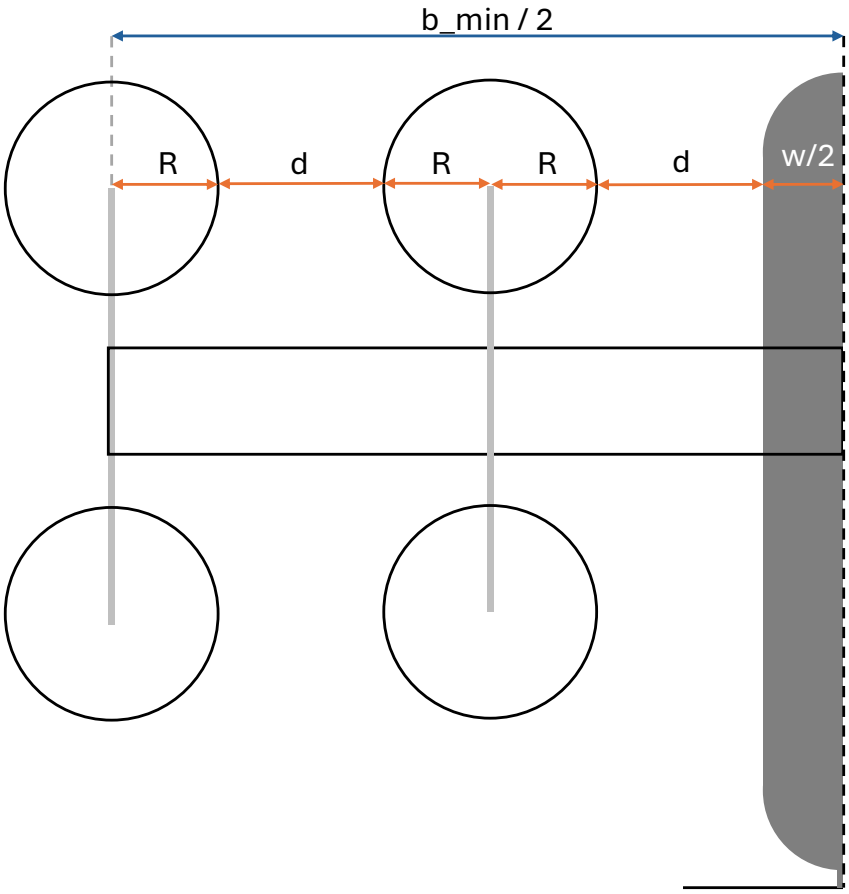


Figure 12: Geometry constraint on minimal wing span, lifting rotor and fuselage interference

### 7.3 Vertipad Constraint

Since the construction of new vertiports involves considerable financial investment and in many cases complex authorization procedures, a successful initial eVTOL operation can be planned on the basis of a design that meets the requirements of existing heliports. According an author-led expert interview with the helipad data provider "Helipaddy", the average $D$-value for existing helipads, potentially be used for UAM-operations, can be assumed for 15m. Therefore, this is assumed to be the maximum dimension of the EVTOL to maximize the likelihood of successful integration into existing air traffic infrastructure. This constraint is expressed in the following equations, where $R_{prop_{hover}}$ is the lifting rotor radius, $d$ is the distance between lifting rotors and fuselage, $w$ is the width of the fuselage, $b$ is the eVTOL wing span:

$$\text{Vertiport Constraint: } 18 \geq 2 \cdot (2 \cdot d + 4 \cdot R_{prop_{hover}} + \frac{w}{2}) \tag{111}$$

$$\text{Vertiport Constraint: } 15 \geq b \tag{112}$$

Within the demonstrated framework it is assumed that the horizontal rotor spacing is $d = 0.2m$ and the fuselage width $w = 1.5m$. Fig. 13 illustrates the D-value, defined by EASA, Ref. [33], as the minimum space needed for an eVTOL to land, taxi, and park. If an eVTOL's D-value exceeds the as average assumed 15m, it may not fit within existing heliports, necessitating larger or specially designed vertiports. This will impacts the design and adaptability of vertiport infrastructure.

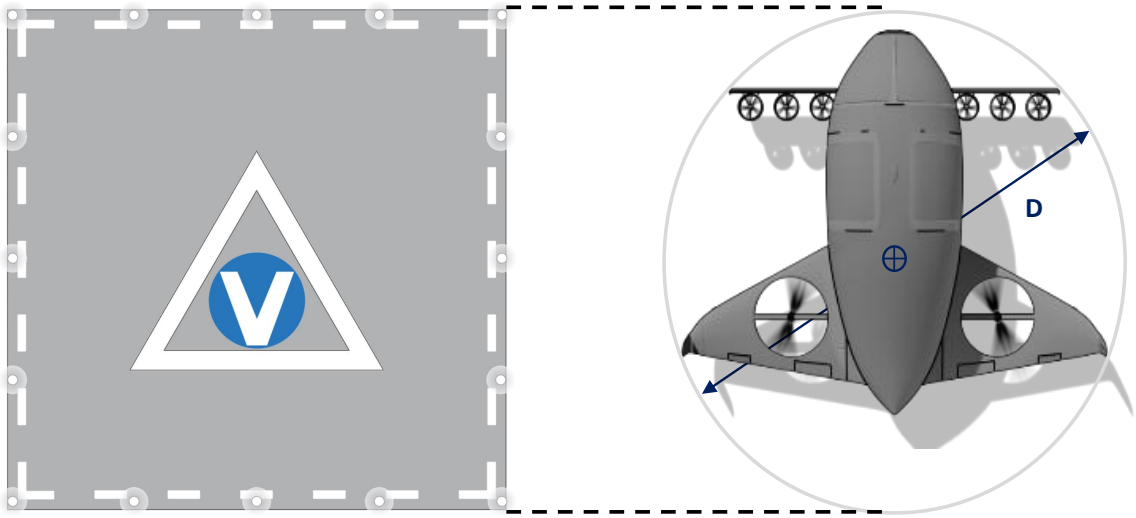


Figure 13: D-value for Vertiports, from Ref. [33].

# 8 Optimization Algorithm Analysis

## 8.1 Scope

This section outlines the employed gradient-based optimization approach and compares it to an alternative gradient-free method. The goal is to provide a clear justification for the chosen optimizer by evaluating its performance and suitability for the problem context.

## 8.2 Gradient-based Algorithm (GBA)

A gradient-based optimization (GBO) approach is used, implemented via the `SLSQP` (Sequential Least Squares Programming) algorithm from Python's `scipy.optimize.minimize`. This method efficiently handles smooth nonlinear objectives and inequality constraints. Design variables are normalized to the $[0,\ 1]$ range to improve numerical stability. To mitigate sensitivity to local minima, a multi-start strategy is applied, where the algorithm is run from multiple random initial points. Optimization options include a gradient step size (`eps = 0.018`), function tolerance (`ftol = 1e-6`), and a maximum of 1000 iterations.

## 8.3 Genetic Algorithm (GA)

A population-based genetic algorithm (GA) [11] is employed using the open-source `geneticalgorithm` Python library. The algorithm operates on bounded continuous variables with optimizing the objective function through stochastic evolution. The GA uses a population of 30 individuals and evolves for up to 300 generations to provide a balance between exploration and computational efficiency. Key parameters include a mutation probability of 0.2 to ensure sufficient diversity to escape local optima, a crossover probability of 0.5 for effective mixing of genetic material, and an elitism ratio of 0.01 to preserve the best solutions. A maximum of 30 generations without improvement is set to trigger termination. Constraints are enforced through penalty-based rejection of infeasible candidates.

## 8.4 GBA-GA Comparison

To evaluate and compare optimizer performance, both algorithms are applied to a shared test case of maximizing the transportation comparison Figure of Merit (FoM), as defined in Section 3.1.7. of the main paper. This objective serves as a representative for the optimization performance, as it integrates submodel elements also relevant to other objectives analyzed in the presented work, as cost and environmental impact. Each optimizer is run independently 10 times to assess consistency, efficiency, and solution quality, as illustrated in Table 12 and 13.

Table 12: Gradient-based (SLSQP) results over 10 multi-start runs

| #Run | Valid | Runtime (s) | Multi-start Runtime (s) | #Evaluations | #Iterations | Result |
|---|---|---|---|---|---|---|
| 1 | Yes | 2.2 | 9.2 | 47 | 5 | 5.741 |
| 2 | Yes | 1.2 | 7.5 | 28 | 4 | 5.741 |
| 3 | Yes | 2.0 | 7.8 | 47 | 5 | 5.741 |
| 4 | Yes | 2.7 | 8.4 | 59 | 8 | 5.741 |
| 5 | Yes | 0.9 | 6.5 | 21 | 3 | 5.741 |
| 6 | No | 0.0 | 7.0 | 0 | 0 | N/A |
| 7 | Yes | 2.4 | 8.4 | 50 | 7 | 5.741 |
| 8 | Yes | 1.7 | 8.5 | 40 | 4 | 5.741 |
| 9 | Yes | 1.7 | 9.5 | 39 | 4 | 5.741 |
| 10 | Yes | 3.3 | 9.9 | 55 | 6 | 5.741 |
| $Ø_{valid}$ | 90% | 2.01 | 8.4 | 42.9 | 5.1 | 5.741 |

## 8.5 Conclusion

The gradient-based optimizer demonstrated significantly faster convergence, requiring on average only 2.01 seconds per valid run (or 8.4 seconds including multi-start), compared to 32.27 seconds for the genetic algorithm (GA), making it approximately 4 to 16 times faster depending on setup. GBO also showed higher reliability, achieving feasibility in 90 % of runs versus 70 % for GA, with failures typically caused by constraint violations due to poor initial values or insufficient search refinement. GBO required far fewer function evaluations ($\approx$43 vs. $\approx$3021), see Figure 14, and iterations ($\approx$5 vs. $\approx$151), while consistently converging to the best-known objective value, as shown in Figure 15.

Table 13: Genetic Algorithm (GA) results

| #Run | Valid | Runtime (s) | #Evaluations | #Iterations | Result |
|---|---|---|---|---|---|
| 1 | Yes | 31.9 | 2790 | 139 | 5.722 |
| 2 | Yes | 33.5 | 3170 | 158 | 5.721 |
| 3 | Yes | 35.5 | 3210 | 160 | 5.718 |
| 4 | Yes | 24.4 | 2270 | 113 | 5.696 |
| 5 | No | 14.9 | 650 | 32 | N/A |
| 6 | No | 13.7 | 650 | 32 | N/A |
| 7 | No | 17.7 | 650 | 32 | N/A |
| 8 | Yes | 34.4 | 3610 | 180 | 5.733 |
| 9 | Yes | 42.5 | 3970 | 198 | 5.729 |
| 10 | Yes | 23.7 | 2130 | 106 | 5.686 |
| $Ø_{valid}$ | 70% | 32.27 | 3021.43 | 150.57 | 5.715 |

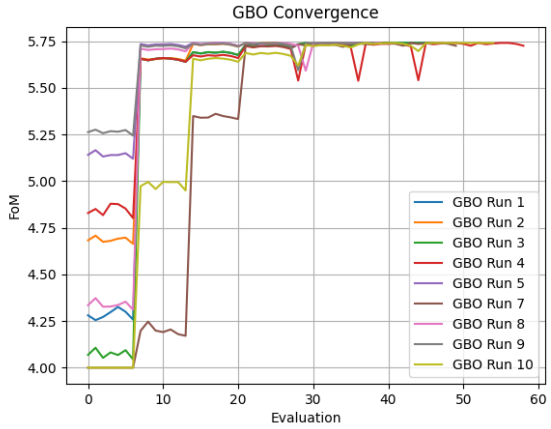


(a) Convergence of valid Gradient-Based Optimization runs.

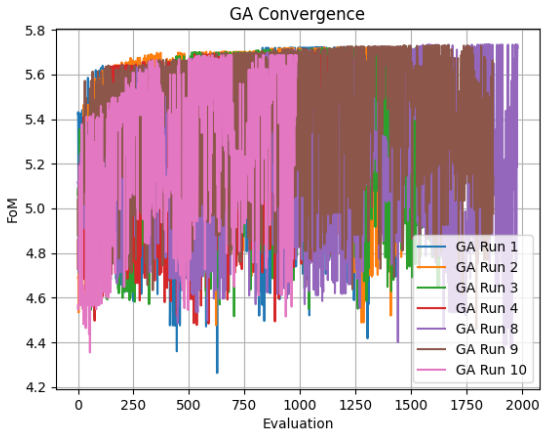


(b) Convergence of valid Genetic Algorithm runs.

Figure 14: Comparison of optimization performance between GA and GBO, illustrating objective function over function evaluations.

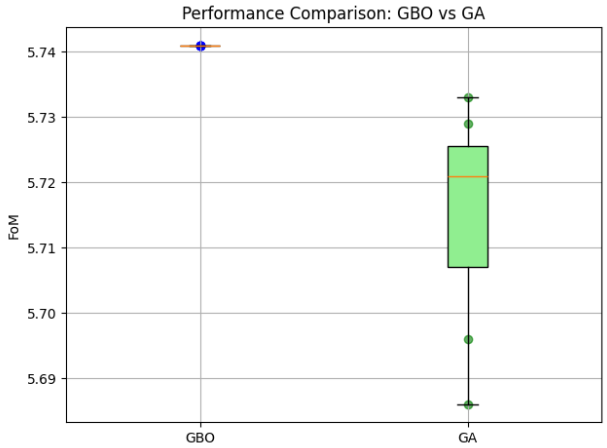


Figure 15: Boxplot comparison of FoM results from valid GBO and GA runs.

These results highlight the robustness and efficiency of the selected gradient-based approach for the presented design problem. Nonetheless, GA remains a viable tool for broad design space exploration and may be useful for generating high-quality initial guesses to seed gradient-based optimization.

## References


[1] European Union Aviation Safety Agency. Special condition vtol. Available online: https://www.easa.europa.eu/en/document-library/product-certification-consultations/special-condition-vtol, 2024. Accessed: 2024-06-12.

[2] European Union Aviation Safety Agency. EASA review of standard passenger weights 2022 shows no significant change. Available online: https://www.easa.europa.eu/en/newsroom-and-events/news/easa-review-standard-passenger-weights-2022-shows-no-significant-change, 2022. Accessed: 2024-06-12.

[3] Daniel P. Raymer. *Aircraft Design: A Conceptual Approach*. AIAA Education Series. American Institute of Aeronautics and Astronautics, 2nd edition, 1992.

[4] Snorri Gudmundsson. *General Aviation Aircraft Design: Applied Methods and Procedures*. Butterworth-Heinemann, 2013. Accessed: 2024-08-08.

[5] Shugo Kaneko and Joaquim R.R.A. Martins. Simultaneous optimization of design and takeoff trajectory for an evtol aircraft. *Aerospace Science and Technology*, 155:109617, 2024.

[6] MT-Propeller. Technical Data Sheets for MTV Series Propellers.

- MTV-11: https://www.mt-propeller.com/pdf/TCDS_EASA/MTV-11.pdf
- MTV-15: https://www.mt-propeller.com/pdf/TCDS_EASA/MTV-15.pdf
- MTV-17: https://www.mt-propeller.com/pdf/TCDS_EASA/MTV-17.pdf
- MTV-20: https://www.mt-propeller.com/pdf/TCDS_EASA/MTV-20.pdf
- MTV-21: https://www.mt-propeller.com/pdf/TCDS_EASA/MTV-21.pdf

, 2023. Accessed: August 10, 2024.

[7] European Union Aviation Safety Agency (EASA). Easy Access Rules for Large Aeroplanes (CS-25)-CS 25.925. Available online: https://www.easa.europa.eu/en/document-library/easy-access-rules/online-publications/easy-access-rules-large-aeroplanes-cs-25?kw=propeller%20clearance, note = Accessed: August 10, 2024, 2024. Accessed: August 10, 2024.

[8] Federal Aviation Administration. 14 cfr § 25.925 - propeller clearance. Available online: https://www.ecfr.gov/current/title-14/chapter-I/subchapter-C/part-25/subpart-E/subject-group-ECFR3db216ad9d52259/section-25.925, 2024. Accessed: August 10, 2024.

[9] B. Govindarajan and A. Sridharan. Conceptual sizing of vertical lift package delivery platforms. *Journal of Aircraft*, 57(6):1170, 2020.

[10] Carlos Silva, Wayne Johnson, Ken Antcliff, and Michael D. Patterson. Vtol urban air mobility concept vehicles for technology development, 2018.

[11] Joaquim R. R. A. Martins and Andrew Ning. *Engineering Design Optimization*. Cambridge University Press, 2021.

[12] S. S. Chauhan and J. R. R. A. Martins. Tilt-wing evtol takeoff trajectory optimization. *Journal of Aircraft*, 57(1):93, 2019.

[13] Airfoil Tools. Naca airfoil polars (naca 0012, naca 2412). Available online: NACA 0012 (http://airfoiltools.com/polar/details?polar=xf-n0012-il-200000), NACA 2412 (http://airfoiltools.com/polar/details?polar=xf-naca2412-il-200000), 2024. Accessed: 2024-07-16.

[14] Alessandro Bacchini, Enrico Cestino, Benjamin Van Magill, and Dries Verstraete. Impact of lift propeller drag on the performance of evtol lift+cruise aircraft. *Aerospace Science and Technology*, 109:106429, 2021.

[15] Mark Drela. Xfoil: An analysis and design system for low reynolds number airfoils, 1989.

[16] A. Brown and W. L. Harris. A vehicle design and optimization model for on-demand aviation. *AIAA/ASCE/AHS/ASC Structures, Structural Dynamics, and Materials Conference*, 2018.

[17] Chi Yang, Yuchen Gao, Weigang Wei, Chang Liu, Kai Wang, Yue Zhang, Haiping Liu, Xiaoqing Lu, Fei Ren, Yuyi Yang, Kejie Li, and Xinfeng Zhao. Challenges and key requirements of batteries for electric vertical takeoff and landing aircraft. *Joule*, 5(8):1884–1900, 2021. Accessed: 2024-06-12.

[18] Constantin Rotaru and Michael Todorov. *Helicopter Flight Physics*. IntechOpen, February 2018. Licensed under CC BY 4.0.

[19] James F. Marchman III. *Altitude Change: Climb and Glide*, chapter 5. James F. Marchman III in association with the University Libraries at Virginia Tech, 2021.

[20] Jeff Holden and Nikhil Goel. Fast-forwarding to a future of on-demand urban air transportation. Available online: https://evtol.news/__media/PDFs/UberElevateWhitePaperOct2016.pdf, 2016.

[21] H. B. Faulkner. The ata-67 formula for direct operating cost. Available online: https://ntrs.nasa.gov/api/citations/19730024119/downloads/19730024119.pdf, May 1973. NASA Technical Memorandum.

[22] Y. Mihara, P. Pawnlada, A. Nakamoto, T. Nakamura, M. Nakano, and P. Pawnlanda. Cost analysis of evtol configuration design for an air ambulance system in japan. *Journal of Advanced Transportation*, 2021:Article ID 8821234, 2021. Available online.

[23] DFS Deutsche Flugsicherung. Charges - legal framework. Available online: https://www.dfs.de/homepage/en/air-traffic-control/legal-framework/charges/, 2024. Accessed: 2024-06-15.

[24] Economic Research Institute (ERI). Helicopter pilot salary in germany. Available online: https://www.erieri.com/salary/job/helicopter-pilot/germany#:~:text=The%20average%20salary%20range%20for,conducted%20and%20researched%20by%20ERI., 2024. Accessed: 2024-06-15.

[25] Investopedia. Annuity method of depreciation. https://www.investopedia.com/terms/a/annuity-method-of-depreciation.asp#:~:text=The%20annuity%20method%20of%20depreciation%20is%20a%20process%20used%20to,least%20constant)%20rate%20of%20return., 2023. Accessed: 2024-06-15.

[26] Valor International. Orders for eve's flying car total $8.3bn. Available online: https://valorinternational.globo.com/business/news/2023/05/02/orders-for-eves-flying-car-total-83bn.ghtml, 2023. Accessed: 2024-06-15.

[27] International Civil Aviation Organization (ICAO). Airlines operating costs and productivity. Available online: https://www.icao.int/mid/documents/2017/aviation%20data%20and%20analysis%20seminar/ppt3%20-%20airlines%20operating%20costs%20and%20productivity.pdf, 2017. Accessed: 2024-06-16.

[28] Taxi fare calculator london. https://www.bettertaxi.com/taxi-fare-calculator/london/. Accessed: 2024-08-19.

[29] Michael J. Duffy, Sean Wakayama, Ryan Hupp, Roger Lacy, and Matt Stauffer. A study in reducing the cost of vertical flight with electric propulsion. In *American Institute of Aeronautics and Astronautics Conference*. The Boeing Company, 2017. Accessed: 2024-08-13.

[30] Chris Wetherell. Let's talk about the panasonic ncr18650b. Available online: https://turtleherding.com/wp-content/uploads/2018/06/Lets-talk-about-the-Panasonic-NCR18650B.pdf, 2018. Accessed: 2024-08-13.

[31] R. Schlegel and R. King and H. Mull. Helicopter Rotor Noise Generation and Propagation. Available online: https://apps.dtic.mil/sti/tr/pdf/AD0645884.pdf, October 1966.

[32] T. H. Ha, K. Lee, and J. T. Hwang. Large-scale design-economics optimization of evtol concepts for urban air mobility, 2019. 10.2514/6.2019-1218.

[33] European Union Aviation Safety Agency (EASA). Prototype Technical Specifications for the Design of VFR Vertiports for Operation with Manned VTOL-Capable Aircraft Certified in the Enhanced Category (PTS-VPT-DSN). Available online: https://www.easa.europa.eu/en/document-library/general-publications/prototype-technical-design-specifications-vertiports, March 2022. Non-binding guidance material for vertiport design and operation.